Hindawi
Computational and Mathematical Methods in Medicine
Volume 2022, Article ID 6154866, 20 pages
https://doi.org/10.1155/2022/6154866

Research Article

Stability Analysis and Optimal Control Strategies of an Echinococcosis Transmission Model

Run Yang, Jianglin Zhao, and Yong Yan

Faculty of Science and Technology, Sichuan Minzu College, Kangding, China

Correspondence should be addressed to Jianglin Zhao; ws05101162@163.com

Received 17 March 2022; Revised 29 April 2022; Accepted 1 May 2022; Published 23 May 2022

Academic Editor: Andrei Korobeinikov

This paper presents a deterministic compartmental model for echinococcosis transmission dynamics. The basic reproduction number of the model determines the existence and stability of the disease-free and disease-endemic equilibrium points. We further formulate the optimal control problem and obtain the necessary conditions to minimize the number of infected individuals and the associated costs. Numerical simulations show that optimal control strategies can significantly reduce the number of infected individuals to lower levels. Environmental disinfection may be essential for the elimination of infections. The results of this study will be beneficial for the prevention and control of echinococcosis in the Ganzi Tibetan Autonomous Prefecture and other areas of China.

1. Introduction

Human echinococcosis is a parasitic zoonosis caused by infection with the larval stage of the tapeworm Echinococcus. Note that more than 1 million people are affected with echinococcosis at any one time, and human echinococcosis is often expensive and complicated to treat and may require extensive surgery and prolonged drug therapy [1]. As a result, human echinococcosis poses a significant burden on patients and health care. The life cycle of Echinococcus consists of three stages: egg, larva, and adult (see [2–6]). Adults reside in the definitive hosts (mainly dogs), produce eggs that are passed in the feces, contaminate the environment (for example, water, dog's fur, vegetables, grass, and soil), and are immediately infectious. After ingestion by the intermediate host (mainly sheep, goats, and cattle), Echinococcus eggs (EEs) hatch and release six-hooked oncospheres which migrate into various organs (especially the liver and lung) and then develop into a hydatid cyst. The definitive hosts ingest the cyst-containing organs of the infected intermediate hosts and become infected. The protoscolices begin to develop into adult stages. Humans are accidental intermediate hosts because they acquire the infection in the same way as other intermediate hosts but without the biological contribution of spreading the infection to the definitive hosts. For more related knowledge about echinococcosis, please refer to [1, 2].

Wang et al. [7] developed a deterministic compartment model of echinococcosis transmission and pointed out that the strict slaughter inspection with regard to meat inspection and offal disposal, dog anthelmintics, and public health education about hygiene and dog contact could effectively reduce the spread of echinococcosis. Wu et al. [8] stressed that human inventions (deworming EEs and killing wild dogs) could be the most effective way to control the spread of echinococcosis. Rong et al. [9] showed that promoting public health education and disposing of stray dogs could

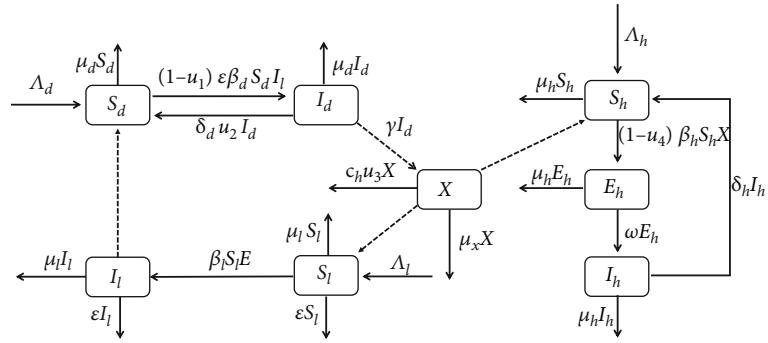

Figure 1: Schematic diagram of the transmission dynamics of Echinococcus.

Table 1: Description of parameters of model (1).

Parameters	Interpretation	Units	Source
Λ_d	Recruitment rate of dogs	21.1×10^4 year^{-1}	Estimated
β_d	Transmission rate from livestock to dogs	5.8×10^{-8} year^{-1}	[7]
μ_d	Natural death rate of dogs	0.08 year^{-1}	[7]
δ_d	Recovery rate of infected dogs	0.21 year^{-1}	Estimated
γ	Released rate from infected dogs	9.7 year^{-1}	[7]
μ_x	Death rate of EEs	1 year^{-1}	[8]
c_h	Disinfection-induced EE mortality rate	10 year^{-1}	Assumed
Λ_l	Recruitment rate of livestock	54.33×10^4 year^{-1}	Estimated
β_l	Infection rate of livestock by ingesting EEs	7.4×10^{-8} year^{-1}	[7]
ε	Fraction of home-slaughtered livestock	0.189	Estimated
μ_l	Natural death rate of livestock	0.152 year^{-1}	[9]
Λ_h	Recruitment rate of humans	1.03×10^4	[29]
β_h	Infection rate of humans by ingesting EEs	4.2×10^{-11} year^{-1}	[7]
ω	Reciprocal of human incubation period	1/14 year^{-1}	[7]
μ_h	Natural death rate of humans	0.0139 year^{-1}	Estimated
δ_h	Recovery rate of humans	0.041 year^{-1}	Estimated
$u_1(t)$	Effectiveness of home slaughter inspection	0–1	Assumed
$u_2(t)$	Effectiveness of anthelmintic treatment	0–1	Assumed
$u_3(t)$	Effectiveness of environmental disinfection	0–1	Assumed
$u_4(t)$	Effectiveness of health education	0–1	Assumed

significantly help control echinococcosis spreading. Hassan and Munganga [10] emphasized that treating red foxes only or disinfecting the environment alone will not be adequate to eradicate the parasite from the community, and a combination of both control strategies would be more effective in controlling the transmission of the disease in the population. Zhu et al. [11] suggested that the low evacuation rate and high mortality rate of EEs could contribute to a significant reduction in human infection cases. Furthermore, they noted that keeping humans away from EEs and enhancing treatment rates would be highly effective in preventing echinococcosis transmission in humans. Tamarozzi et al. [12] confirmed that environmental contamination, particularly through hand-to-mouth transmission, might be of primary importance from an overall appraisal of published literatures. Craig et al. [13] said that the five key elements, preventing dogs from accessing offal, treating dogs with dewormers, meat inspection, no home slaughter, and health education on hygiene and dog contact, are still valid for reducing the spread of echinococcosis today. Zhao and Yang [14] stated that optimal control strategies aimed at minimizing the number of infected individuals and the associated costs could effectively reduce the transmission of echinococcosis.

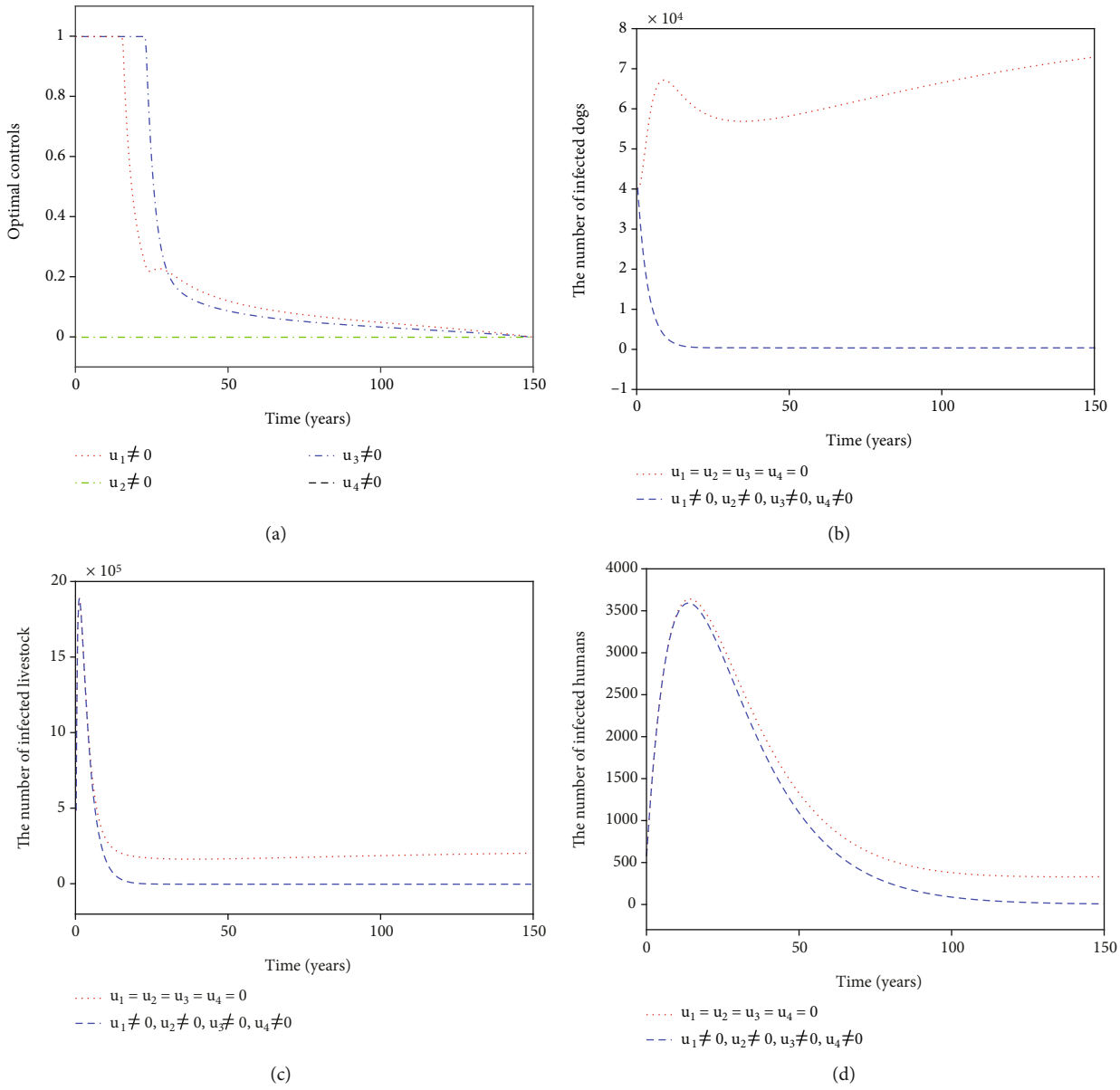

FIGURE 2: Simulation results for Strategy A: (a) depicts the profiles of optimal controls u_1^* and u_2^*; (b–d) represent the number of infected dogs, infected livestock, and infected humans, respectively.

Hassan and Munganga [10] stated that the joint control is more effective than the single one. Thus, the optimal problem of control measures is a worthwhile discussion since the optimal control strategies could reduce the number of infected individuals at the lowest cost level (see [14–21] for example). Although humans are accidental intermediate hosts and do not participate in the life cycle of Echinococcus, once a person becomes infected with the disease, it will place a significant burden on their health and finances. According to [14], we will consider human infection with echinococcosis in our modeling and discuss optimal control strategies by controlling the intensity of deworming, frequency of environmental disinfection, level of strict slaughter inspection, and frequency of health education.

The rest of this paper is organized as follows. In Section 2, a dynamical model of echinococcosis transmission with control is given. A mathematical analysis of the model is presented in Section 3. The optimal control problem is formulated, and the necessary conditions are given in Section 4. Numerical simulations are shown to explore the optimal controls in Section 5. A conclusion and discussion are given in Section 6.

2. Model Formulation

For the dog population, the definitive hosts are divided into two classes: susceptible $S_d(t)$ and infected $I_d(t)$. For the livestock population, the intermediate hosts are decomposed

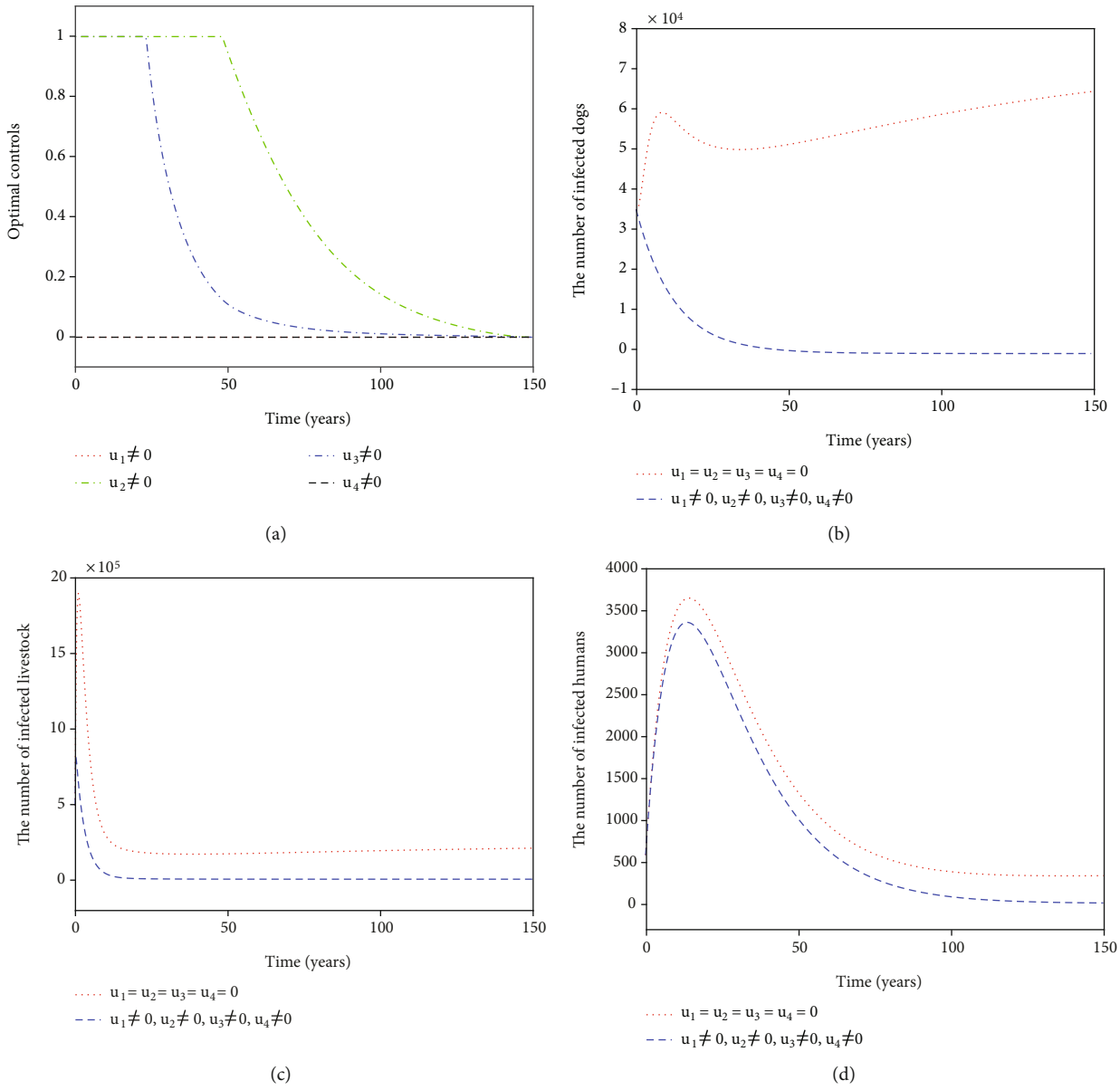

Figure 3: Simulation results for Strategy B: (a) depicts the profiles of optimal controls u_1^* and u_3^*; (b–d) represent the number of infected dogs, infected livestock, and infected humans, respectively.

into susceptible $S_l(t)$ and infected $I_l(t)$. The definitive hosts are infected by ingesting the cyst-containing organs of the infected intermediate hosts. The intermediate hosts become infected by ingesting EEs from their living environment. Humans act as accidental intermediate hosts, acquiring infection when they ingest EEs. The total human population is separated into susceptible $S_h(t)$, exposed $E_h(t)$, and infected $I_h(t)$. The EEs released from the feces of infected dogs are denoted by $X(t)$. A schematic diagram for the dynamical transmission of echinococcosis is demonstrated in Figure 1. Based on this schematic diagram, it has the following transmission model:

$$\begin{cases} \dot{S}_d = \Lambda_d - (1-u_1(t))\varepsilon\beta_d S_d I_l - \mu_d S_d + \delta_d u_2(t) I_d, \\ \dot{I}_d = (1-u_1(t))\varepsilon\beta_d S_d I_l - \mu_d I_d - \delta_d u_2(t) I_d, \\ \dot{X} = \gamma I_d - \mu_x X - c_h u_3(t) X, \\ \dot{S}_l = \Lambda_l - \beta_l S_l X - \varepsilon S_l - \mu_l S_l, \\ \dot{I}_l = \beta_l S_l X - \varepsilon I_l - \mu_l I_l, \\ \dot{S}_h = \Lambda_h - (1-u_4(t))\beta_h S_h X - \mu_h S_h + \delta_h I_h, \\ \dot{E}_h = (1-u_4(t))\beta_h S_h X - \omega E_h - \mu_h E_h, \\ \dot{I}_h = \omega E_h - \mu_h I_h - \delta_h I_h. \end{cases} \tag{1}$$

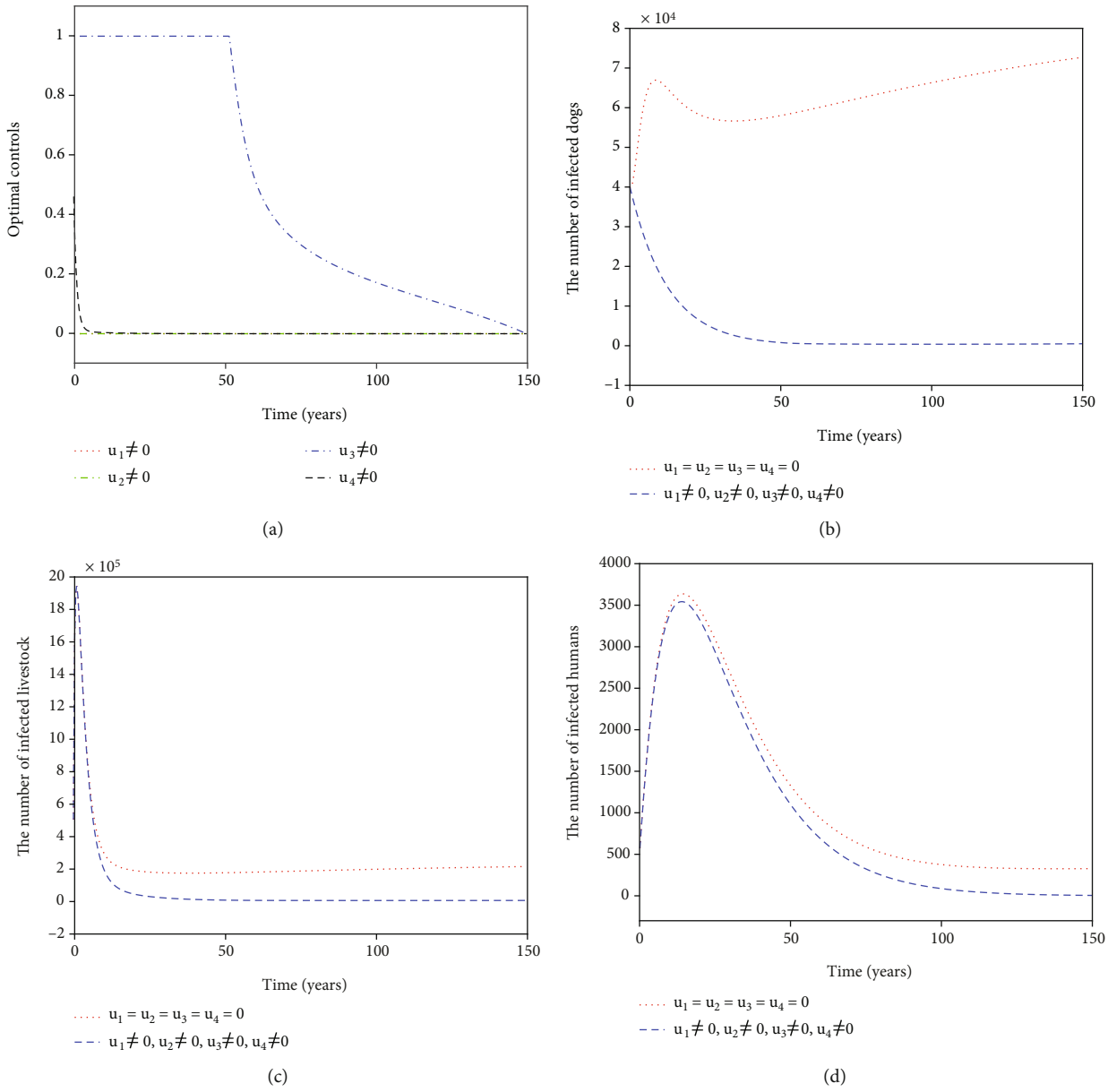

FIGURE 4: Simulation results for Strategy C: (a) depicts the profiles of optimal controls u_1^* and u_4^*; (b–d) represent the number of infected dogs, infected livestock, and infected humans, respectively.

In (1), Λ_d denotes the annual recruitment rate of the susceptible dogs, μ_d is the natural death rate of the dog population, δ_d represents the recovery rate of infectious dogs, and $u_2(t) \in [0, 1]$ is the control on the use of praziquantel (PZQ) dosing for infected dogs. $(1 - u_1(t))\varepsilon\beta_d S_d I_l$ describes the transmission of echinococcosis between susceptible definitive hosts and infectious intermediate hosts, $u_1(t) \in [0, 1]$ is the control on the use of very strict slaughter inspection with regard to meat inspection and offal disposal for livestock, and ε is the home slaughter fraction of livestock. In resource-poor pastoral regions, livestock traditionally pervade home slaughter, so the dog infection rate depends on the home slaughter fraction ε of livestock being available for offal of infected livestock. γ denotes the released rate of EEs by infectious definitive hosts, μ_x accounts for the natural death rate of EEs, c_h is the death rate of EEs because of environmental disinfection, and $u_3(t) \in [0, 1]$ is the control on the use of environmental disinfection for EEs. Λ_l represents the annual recruitment rate of susceptible intermediate hosts, μ_l is the natural death rate of livestock, and $\beta_l S_l X$ depicts the transmission of EEs to livestock by ingesting EEs in the environment. Λ_h is the annual recruitment rate of a susceptible human population, μ_h represents the natural death rate of humans, $(1 - u_4(t))\beta_h S_h X$ describes the transmission of echinococcosis between susceptible humans and an infectious population, and $u_4(t)$ is the control on the use of health education for humans. When ingesting EEs, humans are infected and then undergo an incubation period

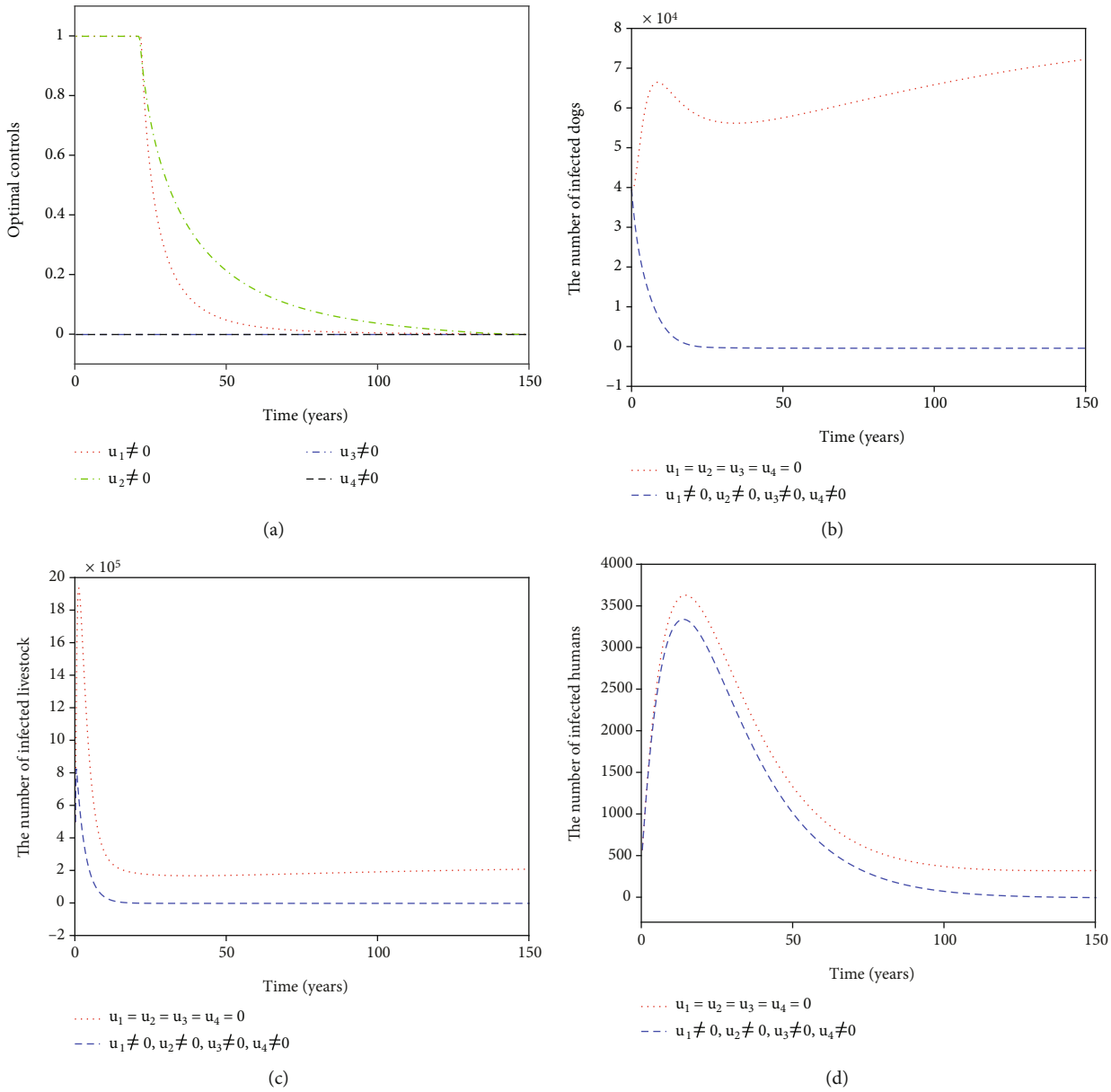

FIGURE 5: Simulation results for Strategy D: (a) depicts the profiles of optimal controls u_2^* and u_3^*; (b–d) represent the number of infected dogs, infected livestock, and infected humans, respectively.

$1/\omega$. The infectious humans recover by an infectious period of mean duration $1/\delta_h$.

3. Model Analysis

When the control variables are considered constant, some mathematical analysis results of model (1) can be obtained.

3.1. Positivity and Boundary of Solutions

Theorem 1.

(i) The solution of model (1) with positive initial conditions is positive for all $t > 0$

(ii) All positive solutions of model (1) with positive initial conditions have the upper boundary in $\mathbb{R}_+^7$

Proof.

(i) Let $(S_d(t), I_d(t), X(t), S_l(t), I_l(t), S_h(t), E_h(t), I_h(t))$ be a solution of model (1) with positive initial values. Define

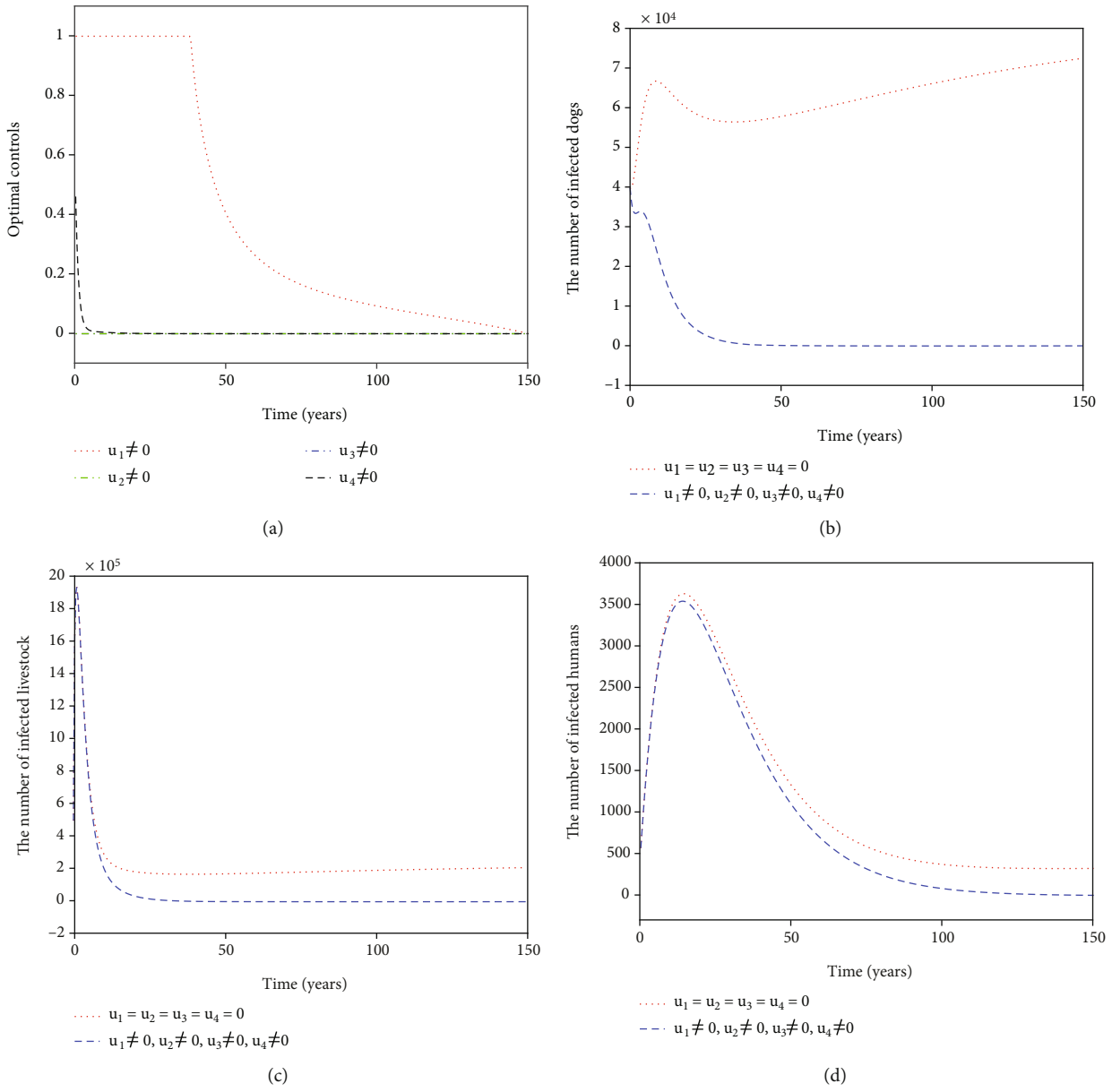

FIGURE 6: Simulation results for Strategy E: (a) depicts the profiles of optimal controls u_2^* and u_4^*; (b–d) represent the number of infected dogs, infected livestock, and infected humans, respectively.

$$t_1 = \sup\{t > 0 : S_d(\tau) > 0, I_d(\tau) > 0, X(\tau) > 0, S_l(\tau) > 0, I_l \cdot (\tau) > 0, S_h(\tau) > 0, E_h(\tau) > 0, I_h(\tau) > 0\}, \tag{2}$$

for all $\tau \in [0, t]$.

Since $\min\{S_d(0), I_d(0), X(0), S_l(0), I_l(0), S_h(0), E_h(0), I_h(0)\} > 0$, then there must be $t_1 > 0$. If $t_1 < \infty$, it gives

$$\min\{S_d(t_1), I_d(t_1), X(t_1), S_l(t_1), I_l(t_1), S_h(t_1), E_h(t_1), I_h(t_1)\} = 0, \tag{3}$$

and $S_d(t) > 0, I_d(t) > 0, X(t) > 0, S_l(t) > 0, I_l(t) > 0, S_h(t) > 0, E_h(t) > 0, I_h(t) > 0$ for all $t \in [0, t_1)$.

On the other hand, the first equation of model (1) could be written as

$$\frac{d}{dt}\left[S_d \exp\left(\int_0^t ((1-u_1)\varepsilon\beta_d I_l + \mu_d)ds\right)\right] = (\Lambda_d + \sigma u_2 I_d)\exp\left(\int_0^t ((1-u_1)\varepsilon\beta_d I_l + \mu_d)ds\right). \tag{4}$$

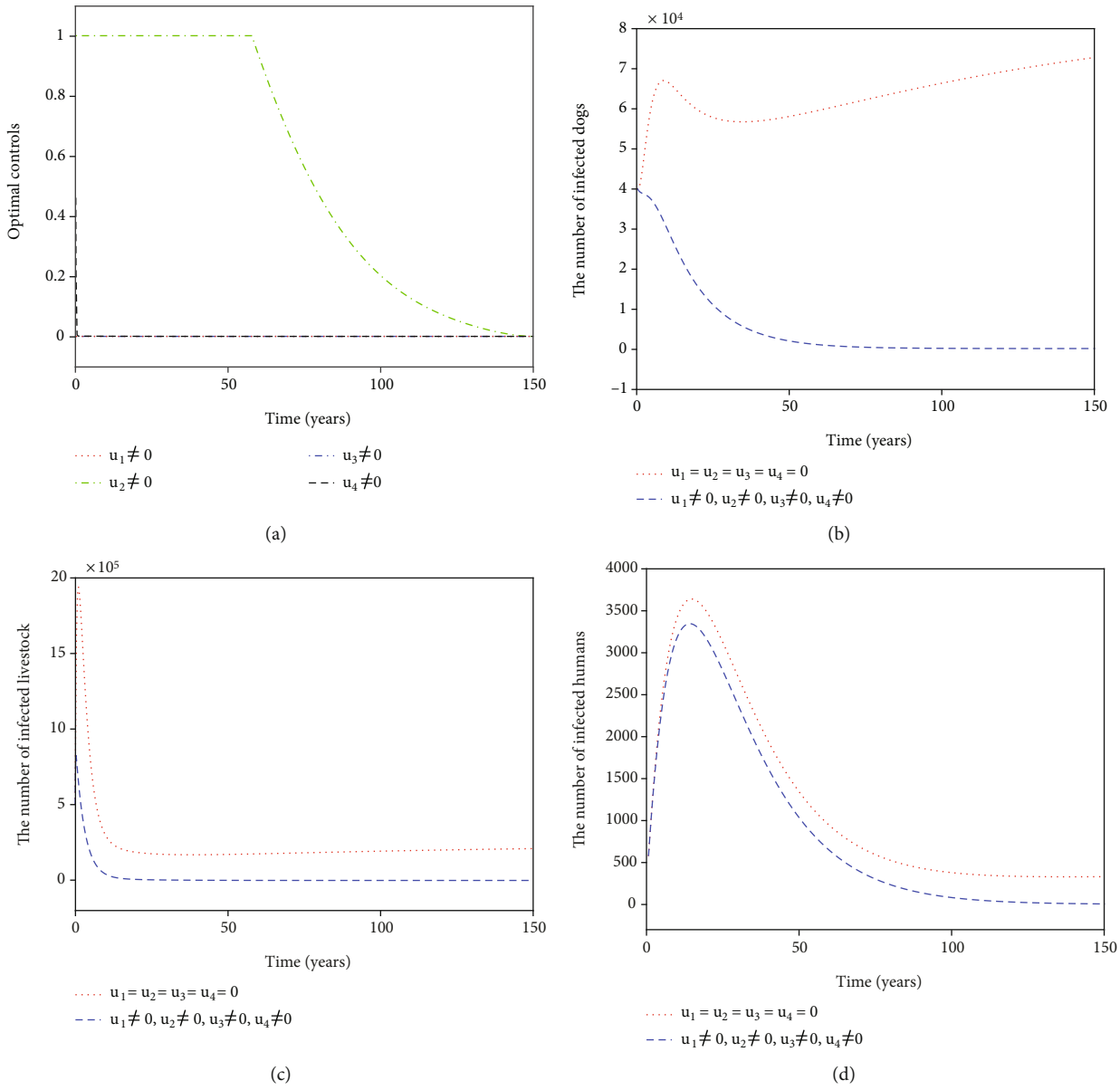

FIGURE 7: Simulation results for Strategy F: (a) depicts the profiles of optimal controls u_3^* and u_4^*; (b–d) represent the number of infected dogs, infected livestock, and infected humans, respectively.

Consequently,

$$S_d(t_1) = S_d(0)\exp\left(-\int_0^{t_1}((1-u_1)\varepsilon\beta_d I_l + \mu_d)dt\right) + \exp\left(-\int_0^{t_1}((1-u_1)\varepsilon\beta_d I_l + \mu_d)dt\right) \times \int_0^{t_1}\left[(\Lambda_d + \sigma u_2 I_d)\left(\exp\left(\int_0^t((1-u_1)\varepsilon\beta_d I_l + \mu_d)ds\right)\right)\right]dt, \quad (5)$$

which implies that $S_d(t_1) > 0$. A similar approach could be applied to show that $I_d(t_1) > 0, S_l(t_1) > 0, I_l(t_1) > 0$ and $E(t_1) > 0$, which is a contradiction. Therefore, $t_1 = \infty$.

Hence, all solutions of model (1) with positive initial conditions remain positive when $t > 0$.

(ii) The first two equations of model (1) could be transformed into

$$\frac{d(S_d + I_d)}{dt} = \Lambda_d - \mu_d(S_d + I_d) \leq \Lambda_d - \mu_d(S_d + I_d). \quad (6)$$

Thus, $\limsup_{t\longrightarrow\infty}(S_d + I_d) \leq \Lambda_d/\mu_d$.

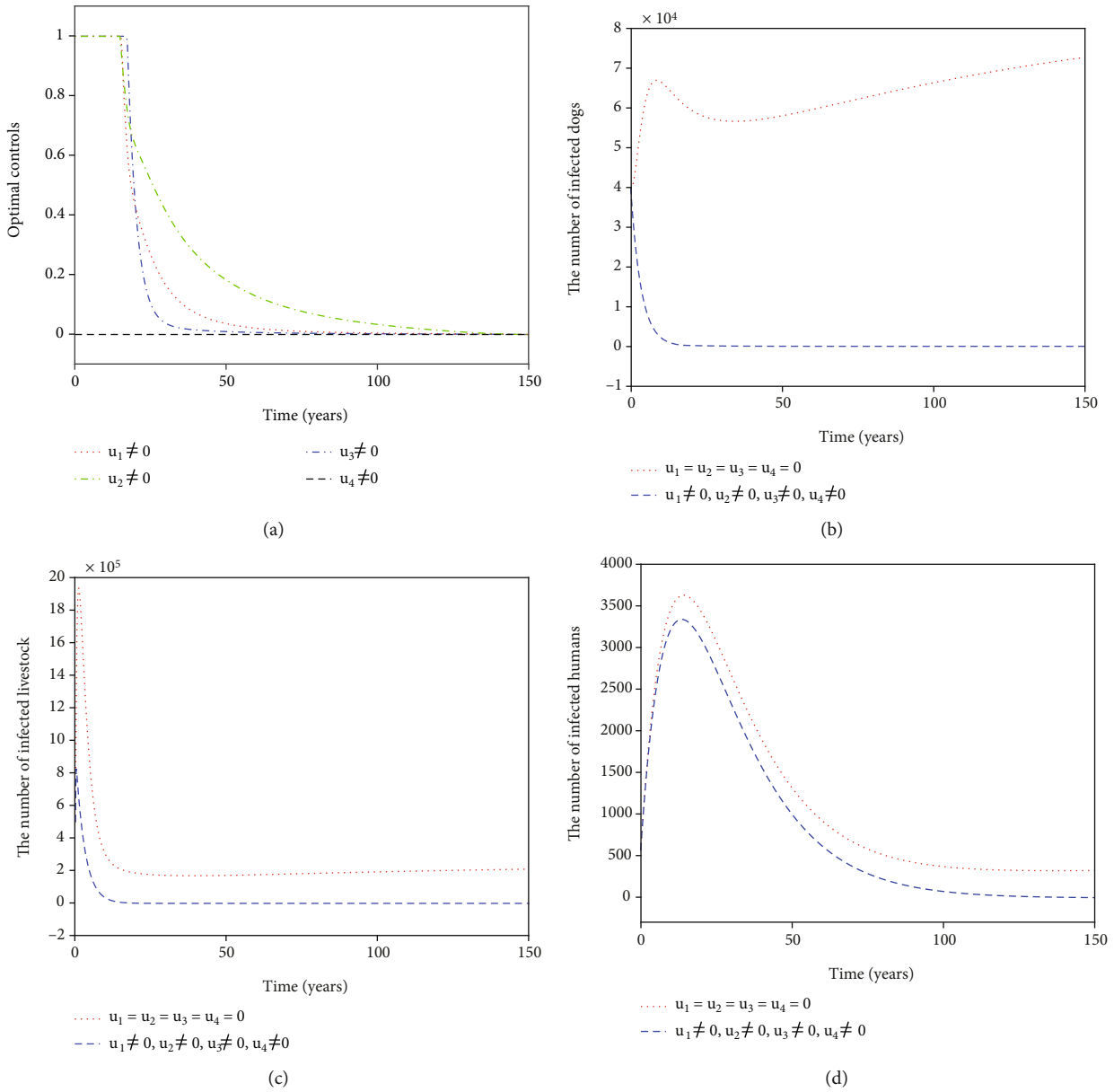

FIGURE 8: Simulation results for Strategy G: (a) depicts the profiles of optimal controls u_1^*, u_2^*, and u_3^*; (b–d) represent the number of infected dogs, infected livestock, and infected humans, respectively.

The fourth and fifth equations of model (1) could be transformed into

$$\frac{d(S_l + I_l)}{dt} = \Lambda_l - (\mu_l + \varepsilon)(S_l + I_l) \leq \Lambda_l - (\mu_l + \varepsilon)(S_l + I_l), \tag{7}$$

which leads to $\limsup_{t \longrightarrow \infty}(S_l + I_l) \leq \Lambda_l/(\mu_l + \varepsilon)$.

The last three equations of model (1) give

$$\frac{d(S_h + E_h + I_h)}{dt} = \Lambda_h - \mu_h(S_h + E_h + I_h) \leq \Lambda_h - \mu_h(S_h + E_h + I_h), \tag{8}$$

which yields $\limsup_{t \longrightarrow \infty}(S_h + E_h + I_h) \leq \Lambda_h/\mu_h$.

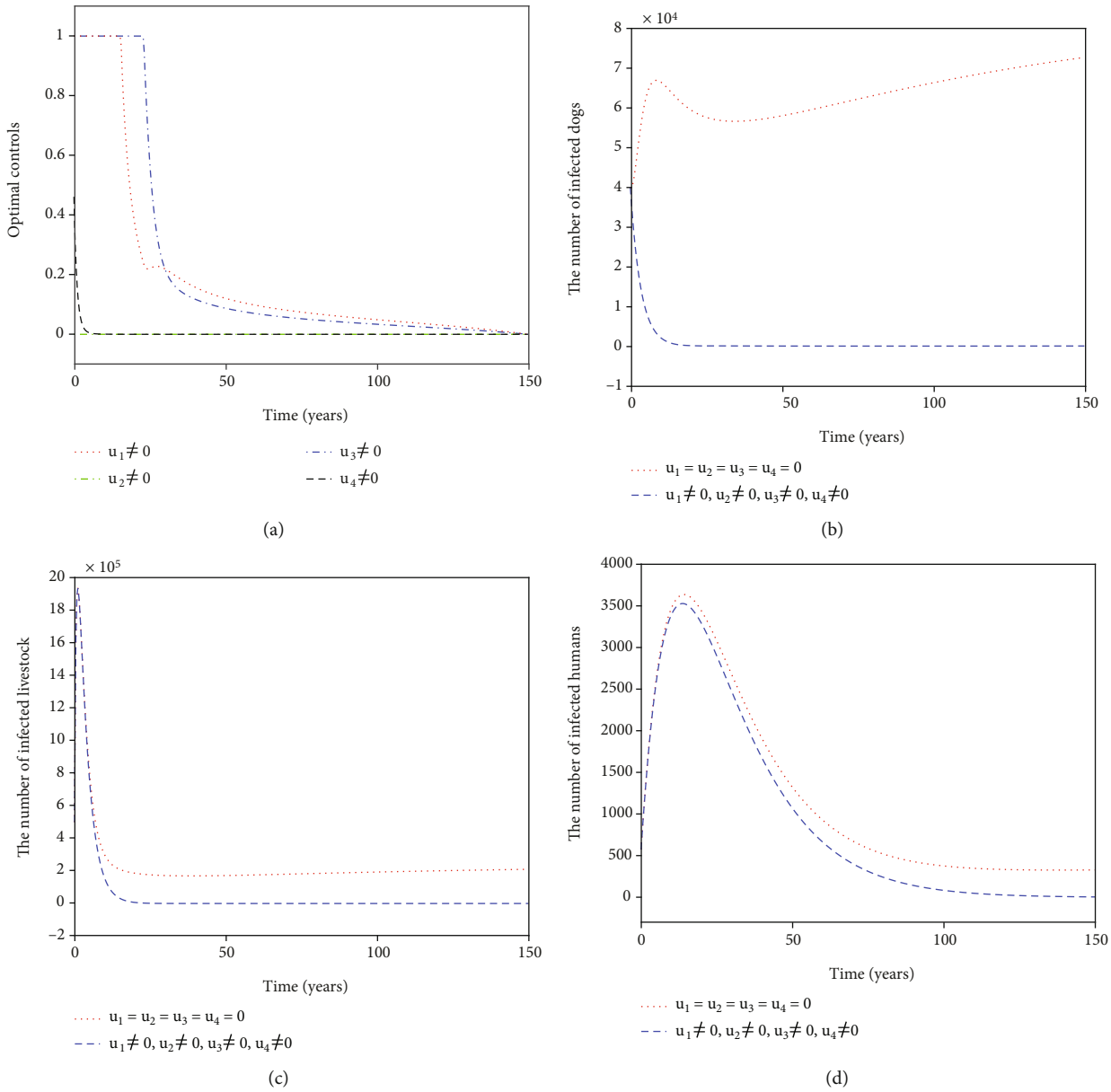

Figure 9: Simulation results for Strategy H: (a) depicts the profiles of optimal controls u_1^*, u_2^*, and u_4^*; (b–d) represent the number of infected dogs, infected livestock, and infected humans, respectively.

From the third equation of model (1), there is

$$\frac{dX}{dt} = \gamma I_d - (\mu_x + c_h u_3)X \le \frac{\gamma \Lambda_d}{\mu_d} - (\mu_x + c_h u_3)X. \quad (9)$$

Hence, $\limsup_{t \longrightarrow \infty} X \le \gamma \Lambda_d / \mu_d (\mu_x + c_h u_3)$.

Let

$$\Gamma = \left\{ (S_d, I_d, E, S_d, I_d, S_h, I_h) \in \mathbb{R}_+^7 : S_d + I_d \le \frac{\Lambda_d}{\mu_d}, X \le \frac{\gamma \Lambda_d}{\mu_d (\mu_e + c_h u_3)}, S_l + I_l \le \frac{\Lambda_l}{\mu_l + \varepsilon}, S_h + E_h + I_h \le \frac{\Lambda_h}{\mu_h} \right\}. \quad (10)$$

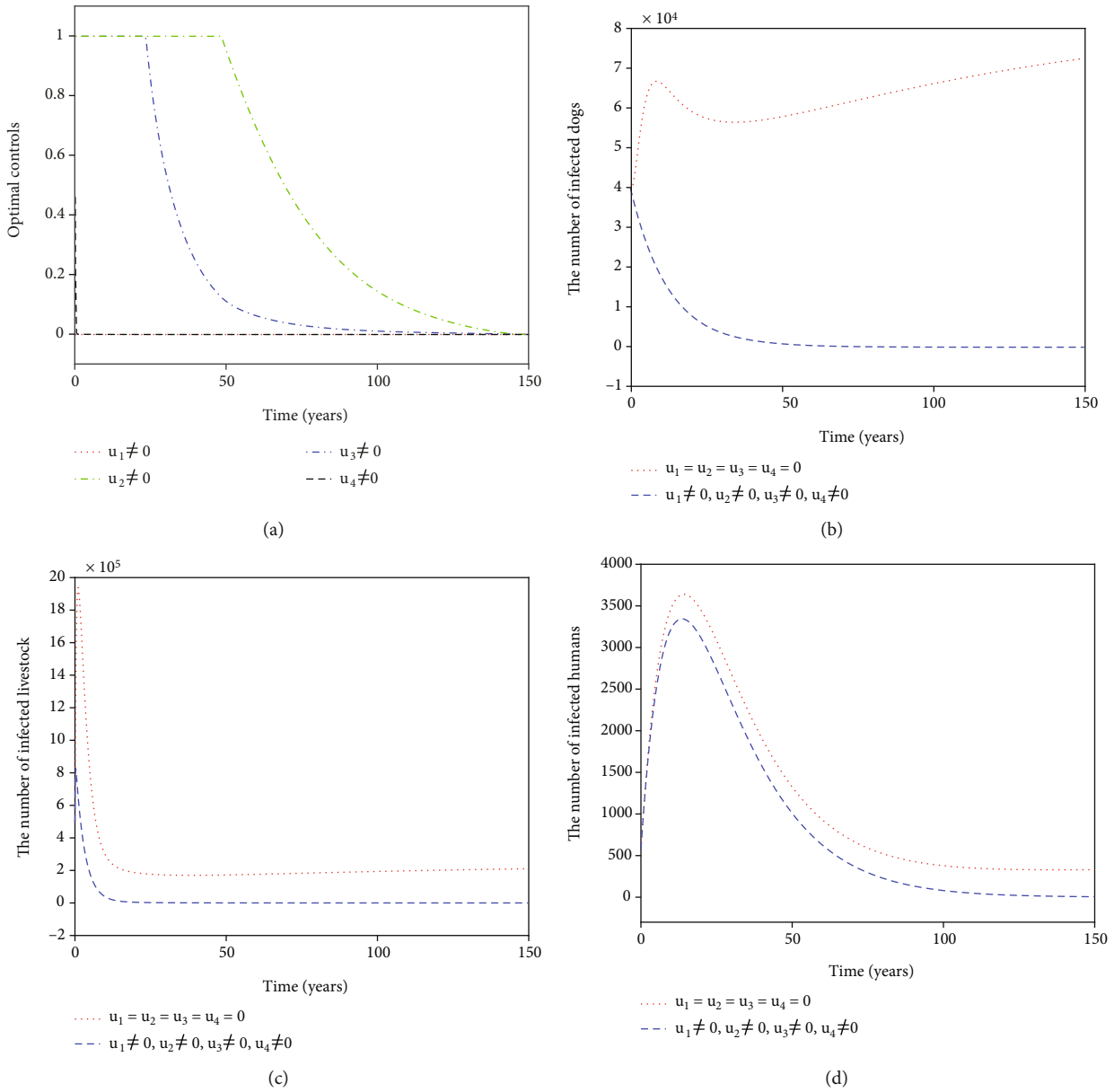

FIGURE 10: Simulation results for Strategy I: (a) depicts the profiles of optimal controls u_1^*, u_3^*, and u_4^*; (b–d) represent the number of infected dogs, infected livestock, and infected humans, respectively.

Thus, all positive solutions of model (1) with positive initial conditions ultimately have the upper boundary in $\mathbb{R}_+^7$. The closed set Γ is positively invariant and attracts the solution to model (1). □

3.2. Equilibrium Points and Stability Analysis. In this section, some mathematical analysis results of model (1) can be obtained when the controls are supposed to be constant.

The disease-free equilibrium of model (1) is denoted by

$$E_{dfe} = \left(S_d^0, 0, 0, S_l^0, 0, S_h^0, 0, 0\right) = \left(\frac{\Lambda_d}{\mu_d}, 0, 0, \frac{\Lambda_l}{\varepsilon + \mu_l}, 0, \frac{\Lambda_h}{\mu_h}, 0, 0\right). \tag{11}$$

In the next, the next-generation matrix approach [22] will be applied for computing the basic reproduction number $\mathcal{R}_0$. The matrix of new infection $\mathcal{F}$ and the matrix of transition $\mathcal{V}$ are defined as follows:

$$\mathcal{F} = \begin{bmatrix} (1-u_1)\varepsilon\beta_d S_d I_l \\ \gamma I_d \\ \beta_l S_l X \\ (1-u_4)\beta_h S_h X \\ 0 \end{bmatrix}, \mathcal{V} = \begin{bmatrix} (\mu_d + \delta_d u_2) I_d \\ (\mu_x + c_h u_3) X \\ (\varepsilon + \mu_l) I_l \\ (\omega + \mu_h) E_h \\ -\omega E_h + (\mu_h + \delta_h) I_h \end{bmatrix}. \tag{12}$$

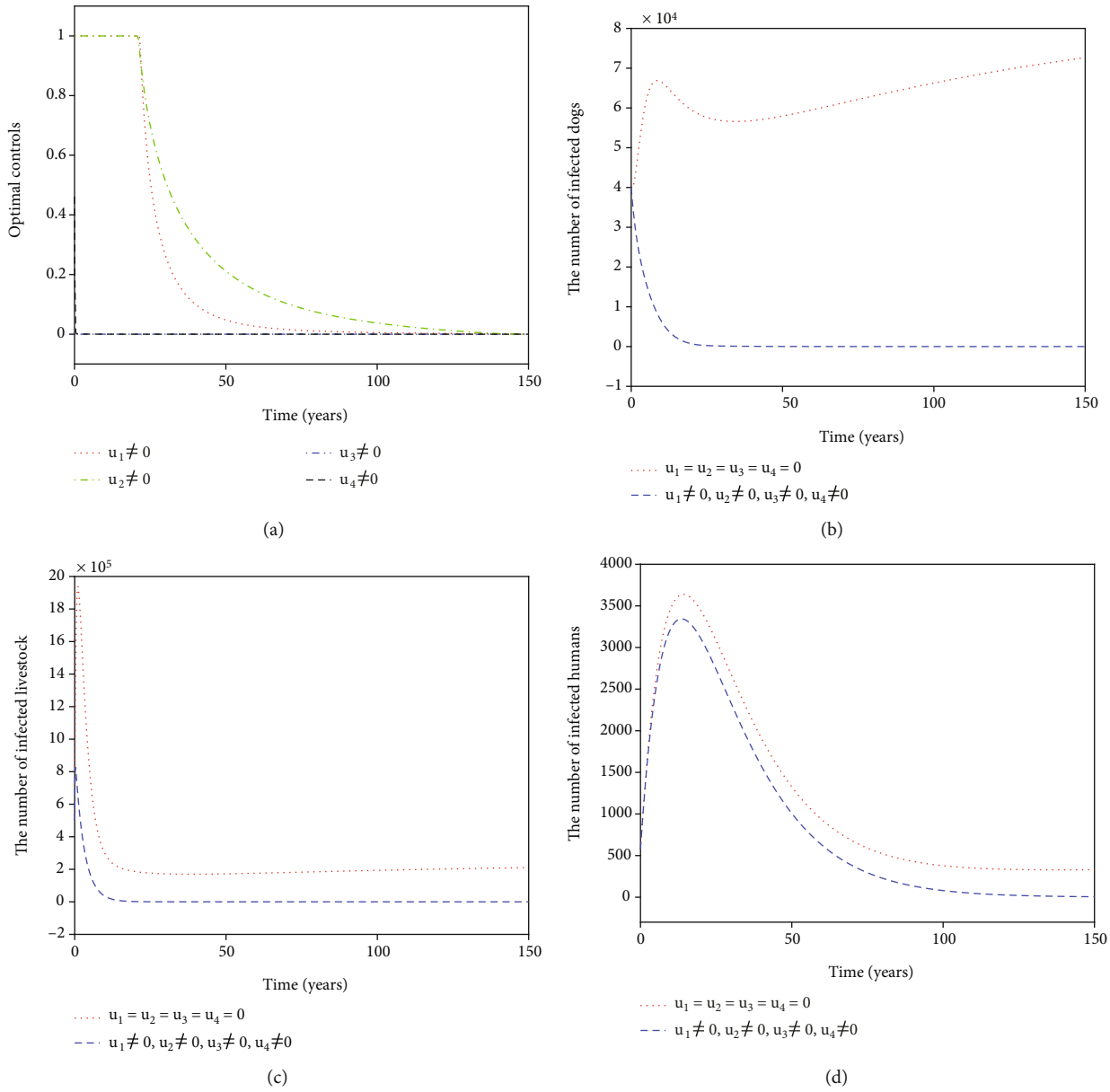

Figure 11: Simulation results for Strategy J: (a) depicts the profiles of optimal controls u_2^*, u_3^*, and u_4^*; (b–d) represent the number of infected dogs, infected livestock, and infected humans, respectively.

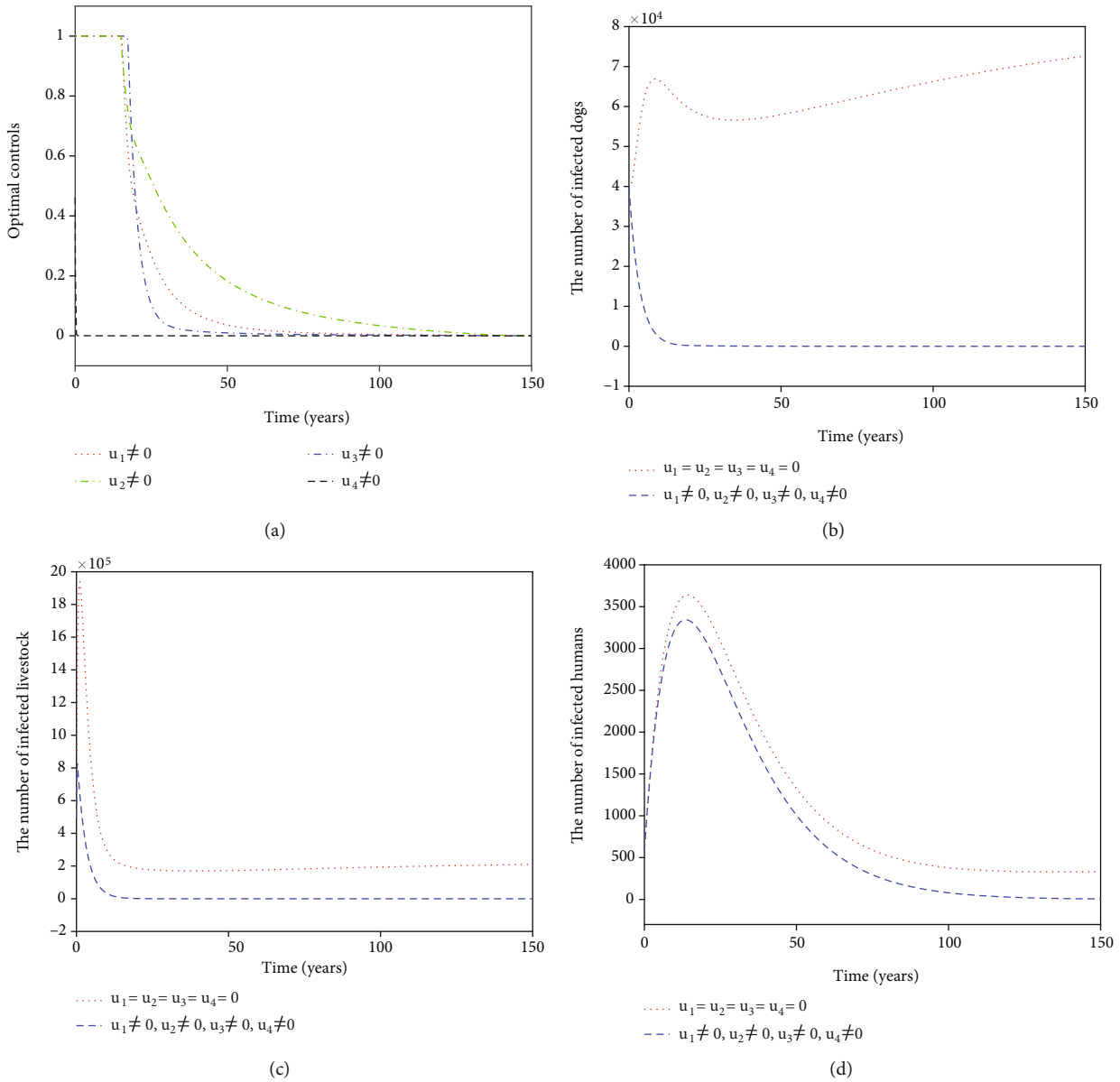

FIGURE 12: Simulation results for Strategy K: (a) depicts the profiles of optimal controls u_1^*, u_2^*, u_3^*, and u_4^*; (b–d) represent the number of infected dogs, infected livestock, and infected humans, respectively.

Furthermore, the Jacobian matrices of $\mathcal{F}$ and $\mathcal{V}$ at the disease-free equilibrium E_{dfe} are, respectively, obtained by

$$F = \begin{bmatrix} 0 & 0 & \frac{(1-u_1)\varepsilon\beta_d\Lambda_d}{\mu_d} & 0 & 0 \\ \gamma & 0 & 0 & 0 & 0 \\ 0 & \frac{\beta_l\Lambda_l}{\varepsilon+\mu_l} & 0 & 0 & 0 \\ 0 & \frac{(1-u_4)\beta_h\Lambda_h}{\mu_h} & 0 & 0 & 0 \\ 0 & 0 & 0 & 0 & 0 \end{bmatrix}, V$$

$$= \begin{bmatrix} \mu_d + \delta_d u_2 & 0 & 0 & 0 & 0 \\ 0 & \mu_x + c_h u_3 & 0 & 0 & 0 \\ 0 & 0 & \varepsilon + \mu_l & 0 & 0 \\ 0 & 0 & 0 & \omega + \mu_h & 0 \\ 0 & 0 & 0 & -\omega & \mu_h + \delta_h \end{bmatrix}. \tag{13}$$

Then, the basic reproduction number that is the largest eigenvalue with a large domain of the next generation matrix FV^{-1} is given by

$$\mathscr{R}_0 = \sqrt[3]{\mathscr{R}_{0x} \cdot \mathscr{R}_{0d} \cdot \mathscr{R}_{0l}}, \tag{14}$$

where

$$\mathscr{R}_{0x} = \frac{\gamma}{\mu_x + c_h u_3}, \mathscr{R}_{0d} = \frac{1}{\mu_d + \delta_d u_2} \cdot \frac{\Lambda_d}{\mu_d} \cdot (1-u_1)\varepsilon\beta_d, \mathscr{R}_{0l} = \frac{1}{\varepsilon + \mu_l} \cdot \frac{\Lambda_l}{\varepsilon + \mu_l} \cdot \beta_l. \tag{15}$$

Here, $\mathscr{R}_{0x}$ denotes the average number of EEs that might be ingested by the intermediate host livestock and humans, $\mathscr{R}_{0d}$ describes the average number of infected dogs by infected livestock, and $\mathscr{R}_{0l}$ accounts for the average number of infected livestock by EEs. For more ecological and epidemiological significance in (14), please refer to [7, 8, 22].

Assume that $E_{ee} = (S_d^*, I_d^*, X^*, S_l^*, I_l^*, S_h^*, E_h^*, I_h^*)$ should be the endemic equilibrium of model (1). Let the right-hand sides of model (1) vanish. By solving these equations, it gives

$$S_d^* = \frac{(\mu_d + \delta_d u_2) I_d^*}{(1-u_1)\varepsilon\beta_d I_l^*}, I_d^* = \frac{\mu_e + c_h u_3}{\gamma} X^*, S_l^* = \frac{\Lambda_l}{\beta_l X^* + \varepsilon + \mu_l},$$

$$I_l^* = \frac{\beta_l S_l^* X^*}{\varepsilon + \mu_l}, X^* = \frac{(\mu_d + \delta_d u_2)(\varepsilon + \mu_l)^2}{\beta_l[(\mu_d + \delta_d u_2)(\varepsilon + \mu_l) + (1-u_1)\varepsilon\beta_d \Lambda_l]} (\mathscr{R}_0^3 - 1),$$

$$S_h^* = \frac{(\omega + \mu_h) E_h^*}{(1-u_4)\beta_h X^*}, I_h^* = \frac{\omega E_h^*}{\mu_h + \delta_h},$$

$$E_h^* = \frac{(1-u_4)\beta_h X^* (\mu_h + \delta_h)\Lambda_h}{\mu_h[(\omega + \mu_h)(\mu_h + \delta_h) + (1-u_4)\beta_h X^* (\omega + \mu_h + \delta_h)]}. \tag{16}$$

Then, it is clear that model (1) has a uniquely endemic equilibrium E_{ee} if and only if $\mathscr{R}_0 > 1$.

A similar method from [7, 9] is used to obtain the following results. Appendix A gives the detailed proof of Theorem 2. In Appendix B, the proof of Theorem 3 is presented. The proof of Theorem 4 can be displayed in Appendix C.

Theorem 2. *The disease-free equilibrium E_{dfe} is locally asymptotically stable if $\mathscr{R}_0 < 1$ and is unstable if $\mathscr{R}_0 > 1$.*

Theorem 3. *The disease-free equilibrium E_{dfe} is globally asymptotically stable if $\mathscr{R}_0 < 1$.*

Theorem 4. *The uniquely endemic equilibrium E_{ee} of model (1) is globally asymptotically stable when $\mathscr{R}_0 > 1$.*

4. Optimal Control

To obtain the optimal control strategies, an objective functional is defined by

$$J(\mathbf{u}) = \int_0^T g(\phi, \mathbf{u}, t)dt = \int_0^T \left[I_d + I_l + I_h + \frac{1}{2}\left(c_1 u_1^2 + c_2 u_2^2 + c_3 u_3^2 + c_4 u_4^2\right)\right] dt, \tag{17}$$

subject to the state system (1). $\phi = (S_d, I_d, X, S_l, I_l, S_h, E_h, I_h)$ is the solution of model (1) with positive initial values and $\mathbf{u} = (u_1(t), u_2(t), u_3(t), u_4(t))$. c_1, c_2, c_3, and c_4 represent the weight constants of the control variables u_1, u_2, u_3, and u_4, respectively. $(1/2)c_1 u_1^2$, $(1/2)c_2 u_2^2$, $(1/2)c_3 u_3^2$, and $(1/2)c_4 u_4^2$ denote the costs of home slaughter inspection, anthelmintic treatment, environmental disinfection, and health education, respectively.

The objective of the optimal control problem (17) is to find a control set that minimizes the infected dogs, the infected livestock, and the infected humans when minimizing the control cost function. Let $\mathbf{U} = \{\mathbf{u} = (u_1(t), u_2(t), u_3(t), u_4(t)): 0 \le u_i(t) \le 1, t \in [0, T], i = 1, 2, 3, 4\}$ be a measurable set. Then, there needs to be the optimal control $\mathbf{u}^* = (u_1^*(t), u_2^*(t), u_3^*(t), u_4^*(t))$ such that

$$J(\mathbf{u}^*) = \min\{J(\mathbf{u}): \mathbf{u} \in U\}. \tag{18}$$

The necessary conditions that determine the optimal control $\mathbf{u}^*$ satisfying (5) with constraint model (1) are derived from Pontryagin's Maximum Principle. Then, the optimal control problem (18) is transformed into minimizing the following Hamiltonian function:

$$H = g(\phi, \mathbf{u}, t) + \sum_{i=1}^{8} \lambda_i f_i(\phi, \mathbf{u}, t), \tag{19}$$

where $f_i(\phi, \mathbf{u}, t)$, $i = 1, 2, 3, 4, 5, 6, 7, 8$, are the right-hand sides of model (1). And λ_i, $i = 1, 2, 3, 4, 5, 6, 7, 8$, are the adjoint variables that satisfy the following costate system:

$$\begin{cases} \dot{\lambda}_1 = -\dfrac{\partial H}{\partial S_d} = (1-u_1)\varepsilon\beta_d I_l(\lambda_1 - \lambda_2) + \lambda_1\mu_d, \\ \dot{\lambda}_2 = -\dfrac{\partial H}{\partial I_d} = -1 - \lambda_1\delta_d u_2 + \lambda_2(\mu_d + \delta_d u_2) - \lambda_3\gamma, \\ \dot{\lambda}_3 = -\dfrac{\partial H}{\partial X} = \lambda_3(\mu_x + c_h u_3) + (\lambda_4 - \lambda_5)\beta_l S_l + (\lambda_6 - \lambda_7)(1-u_4)\beta_h S_h, \\ \dot{\lambda}_4 = -\dfrac{\partial H}{\partial S_l} = \lambda_4(\beta_l X + \varepsilon + \mu_l) - \lambda_5\beta_l X, \\ \dot{\lambda}_5 = -\dfrac{\partial H}{\partial I_l} = -1 + (1-u_1)\varepsilon\beta_d S_d(\lambda_1 - \lambda_2) + \lambda_5(\mu_l + \varepsilon), \\ \dot{\lambda}_6 = -\dfrac{\partial H}{\partial S_h} = (1-u_4)\beta_h X(\lambda_6 - \lambda_7) + \lambda_6\mu_h, \\ \dot{\lambda}_7 = -\dfrac{\partial H}{\partial E_h} = \lambda_7(\omega + \mu_h) - \lambda_8\omega, \\ \dot{\lambda}_8 = -\dfrac{\partial H}{\partial I_h} = -1 - \lambda_6\delta_h + \lambda_8(\delta_h + \mu_h), \end{cases} \tag{20}$$

with boundary conditions $\lambda_i(T) = 0, i = 1, 2, 3, 4, 5, 6, 7, 8$. Additionally, the optimality conditions $\partial H/\partial u_i = 0, i = 1, 2, 3, 4$, lead to the optimal controls:

$$u_i^* = \min\{1, \max\{0, u_i^c\}\}, \quad i = 1, 2, 3, 4, \tag{21}$$

where

$$u_1^c = \frac{\varepsilon\beta_d S_d I_l(\lambda_2 - \lambda_1)}{c_1}, u_2^c = \frac{\delta_d I_d(\lambda_2 - \lambda_1)}{c_2}, u_3^c = \frac{\lambda_3 c_h X}{c_3}, u_4^c = \frac{(\lambda_7 - \lambda_6)\beta_h S_h X}{c_4}. \tag{22}$$

5. Numerical Simulations

In this section, the numerical results of different optimal control scenarios u_1, u_2, u_3, and u_4 are presented. The numerical solution of the optimality system is solved by the forward-backward sweep method [27]. The ode45 solver in MATLAB is used to solve (1) with initial values $S_d(0) = 1.686 \times 10^5$, $I_d(0) = 4 \times 10^4$, $S_l(0) = 3.335 \times 10^6$, $I_l(0) = 5 \times 10^5$, $X(0) = 2 \times 10^7$, $S_h(0) = 8.05 \times 10^5$, $E_h(0) = 8.064 \times 10^3$, and $I_h(0) = 576$, where $S_d(0)$ can be estimated from [28] and $S_l(0), S_h(0), I_h(0)$ can be estimated from [30]. The other initial values of model (1) are assumed. The costate system (20) with boundary conditions $\lambda_i(T) = 0, i = 1, 2, 3, 4, 5, 6, 7, 8$, is numerically obtained from the backward Runge-Kutta scheme. The control variables (21) are updated by entering the new state and adjoint values until the current state; the adjoint and control values are negligibly close. It is well established that the cost of anthelmintic treatment is more expensive than that of environmental disinfection, while the cost of slaughter inspection is cheaper than that of environmental disinfection. On the other hand, the cost of health education is cheaper than that of slaughter inspection. Hence, the weighting constants are considered as $c_1 = 50$, $c_2 = 90$, $c_3 = 70$, and $c_4 = 60$. All other parameters are listed in Table 1. Λ_l is estimated by using the data from the Statistics Bureau of Ganzi Tibetan Autonomous Prefecture [28]. Λ_d, ε, δ_d, and δ_h are estimated by using the data from Zou [30]. The average life expectancy of people in Ganzi Tibetan Autonomous Prefecture (see [29]) was 72.10 years in 2016. Therefore, the natural death rate μ_h of humans in Ganzi Tibetan Autonomous Prefecture is estimated as $\mu_h = 1/72.1 \approx 0.0139$. The death rate of echinococcosis eggs due to environmental disinfection cannot be directly acquired. It is instead assumed that the parasite egg mortality rate induced by environmental disinfection should arrive at ten times higher than the natural death rate. The combined employment of two, three, and four control measures will be studied. The following scenarios are considered:

(A) *Scenario one*: coupled control measures

(i) *Strategy A*: slaughter inspection and anthelmintic treatment (u_1, u_2)

(ii) *Strategy B*: slaughter inspection and environmental disinfection (u_1, u_3)

(iii) *Strategy C*: slaughter inspection and health education (u_1, u_4)

(iv) *Strategy D*: anthelmintic treatment and environmental disinfection (u_2, u_3)

(v) *Strategy E*: anthelmintic treatment and health education (u_2, u_4)

(vi) *Strategy F*: environmental disinfection and health education (u_3, u_4)

(B) *Scenario two*: threefold control measures

(i) *Strategy G*: slaughter inspection, anthelmintic treatment, and environmental disinfection (u_1, u_2, u_3)

(ii) *Strategy H*: slaughter inspection, anthelmintic treatment, and health education (u_1, u_2, u_4)

(iii) *Strategy I*: slaughter inspection, environmental disinfection, and health education (u_1, u_3, u_4)

(iv) *Strategy J*: anthelmintic treatment, environmental disinfection, and health education $(u_2, u_3, u_4$

(C) *Scenario three*: fourfold control measures

(i) *Strategy K*: slaughter inspection, anthelmintic treatment, environmental disinfection, and health education (u_1, u_2, u_3, u_4)

For Strategy A, the slaughter inspection control u_1 and the anthelmintic treatment control u_2 are merely carried out while the environmental disinfection control u_3 and the health education control u_4 are chosen to be ignored. Figure 2(a) shows the paths of optimal controls u_1^* and u_2^*. The slaughter inspection (blue dash-dot line in Figure 2(a)) should be executed 100% for 15 years and then decreases gradually to zero. Meanwhile, the anthelmintic treatment (red dotted line in Figure 2(a)) needs to start the 100% use for 10 years and then declines to zero. Figures 2(b)–2(d) illustrates the effect of the optimal controls u_1^* and u_2^*. When there is no control (see the blue dashed lines in Figures 2(b)–2(d)), the disease is prevalent. However, when the optimal controls are implemented (see the red dotted lines in Figures 2(b)–2(d)), the number of infected dogs, infected livestock, and infected humans could be significantly minimized to the lower level $(I_d, I_l, I_h) = (61,207,6)$. For Strategy B, the slaughter inspection control u_1 and the environmental disinfection control u_3 are merely applied in (17) while the anthelmintic treatment and health education are not considered, i.e., $u_2 = 0, u_4 = 0$. Figure 3(a) presents the profiles of optimal controls u_1^* and u_3^*. The slaughter inspection (blue dash-dot line in Figure 3(a)) is done 100% intensively for 16 years and then decreases gradually till the end of control. Meanwhile, the environmental disinfection control (green dash-dot line in Figure 3(a)) begins with 100% use for 32 years and then declines to zero. Figures 3(b)–3(d) display the effect of u_1^* and u_3^*. It is obvious that there is a

considerable difference in the number of infected dogs, infected livestock, and infected humans between the controlled cases (see the blue dashed lines in Figures 3(b)–3(d)) and the cases without control (see the red dotted lines in Figures 3(b)–3(d)). The number of infected dogs, infected livestock, and infected humans under Strategy B could drop to the lower level $(I_d, I_l, I_h) = (24,61,6)$. For Strategy C, u_1 and u_4 are merely considered in (17) while u_2 and u_3 are ignored. Figure 4(a) shows the profiles of optimal controls u_1^* and u_4^*. The slaughter inspection (blue dash-dot line in Figure 4(a)) is kept at the maximum use of 100% for 34 years and then declines gradually to zero. On the contrary, the health education u_4^* (black dashed line in Figure 4(a)) declines from the maximum use of 46.1% to zero in 16 years. Figures 4(b)–4(d) display that the number of infected dogs, infected livestock, and infected humans could drop to the lower level $(I_d, I_l, I_h) = (319,1070,8)$. For Strategy D, u_2 and u_3 are implemented to optimize the objective functional (17) while $u_1 = 0$ and $u_4 = 0$. Figure 5(a) shows the paths of u_2^* and u_3^*. Both the anthelmintic treatment (red dotted line in Figure 5(a)) and the environmental disinfection (green dash-dot line in Figure 5(a)) should be done 100% intensively for 14 years and then decline gradually to zero. Figures 5(b)–5(d) display that there could exist a considerable significance for reducing the number of infected dogs, infected livestock, and infected humans (blue dashed line) that drops to the lower level $(I_d, I_l, I_h) = (6,16,5)$. For Strategy E, u_2 and u_4 are considered while $u_1 = 0$ and $u_3 = 0$. Figure 6(a) shows the profiles of u_2^* and u_4^*. The control u_2^* (red dotted line in Figure 6(a)) has a 100% use for 25 years and then drops gradually to zero. Meanwhile, the control effort u_4^* (black dashed line in Figure 6(a)) decays from the maximum use of 46.1% to zero in 14 years. Figures 6(b)–6(d) suggest that Strategy E could provide a significant reduction in the number of infected dogs, infected livestock, and infected humans that decreases to the lower level $(I_d, I_l, I_h) = (118,396,7)$. For Strategy F, u_3 and u_4 are considered while $u_1 = 0$ and $u_2 = 0$. Figure 7(a) presents the paths of u_3^* and u_4^*. The control u_3^* (green dash-dot line in Figure 7(a)) needs to perform a 100% use for 39 years and then gradually decreases to zero. Meanwhile, the control u_4^* (black dashed line in Figure 7(a)) drops rapidly from the maximum use of 46.1% to zero in five years. Figures 7(b)–7(d) show that Strategy F could provide a significant reduction in the number of infected dogs, infected livestock, and infected humans that drops to the lower level $(I_d, I_l, I_h) = (35,84,6)$.

For Strategy G, the controls u_1, u_2, and u_3 are considered while $u_4 = 0$. Figure 8(a) shows the paths of u_1^*, u_2^*, and u_3^*. The control u_1^* (blue dash-dot line in Figure 8(a)) has a 100% use for 12 years and then decreases gradually to zero. Both the control u_2^* (red dotted line in Figure 8(a)) and the control u_3^* (green dash-dot line in Figure 8(a)) have a 100% use for 10 years and then drop gradually to zero. Figures 8(b)–8(d) suggest that the number of infected dogs, infected livestock, and infected humans under Strategy G (blue dashed line) could be significantly reduced to a lower level $(I_d, I_l, I_h) = (6,15,5)$ compared to no control (red dotted line). For Strategy H, the controls u_1, u_2, and u_4 are considered while $u_3 = 0$. Figure 9(a) presents the paths of u_1^*, u_2^*, and u_4^*. The slaughter inspection (blue dash-dot line in Figure 9(a)) should be done 100% for 15 years and then decreases gradually to zero. The anthelmintic treatment u_2^* (red dotted line in Figure 9(a)) has the 100% use for 10 years and then declines to zero. On the contrary, the health education u_4^* (black dashed line in Figure 9(a)) drops rapidly from the maximum use of 46.1% to zero in 11 years. Figures 9(b)–9(d) display that there is a significance for u_1^*, u_2^*, and u_4^* reducing the number of infected dogs, infected livestock, and infected humans (blue dashed line) that drops to a lower level $(I_d, I_l, I_h) = (62,207,6)$. For Strategy I, u_1, u_3, and u_4 are implemented in (17) while $u_2 = 0$. Figure 10(a) shows the paths of u_1^*, u_3^*, and u_4^*. The control u_1^* (blue dash-dot line in Figure 10(a)) should be done 100% intensively for 16 years and then declines gradually to zero, while the control u_3^* (green dash-dot line in Figure 10(a)) has the maximum use (100%) for 32 years before dropping gradually to zero. The control u_4^* drops rapidly from the maximum use (46.1%) to zero in five years. Figures 10(b)–10(d) suggest that there could be a considerable significance for reducing the number of infected dogs, infected livestock, and infected humans (blue dashed line) that decreases to a lower level $(I_d, I_l, I_h) = (24,61,6)$. For Strategy J, u_2, u_3, and u_4 are considered while $u_1 = 0$. The optimal controls u_2^*, u_3^*, and u_4^* are presented in Figure 11(a). Both u_2^* (red dotted line in Figure 11(a)) and u_3^* (green dash-dot line in Figure 11(a)) have a 100% use for 14 years and then drop gradually to zero. Meanwhile, u_4^* (black dashed line in Figure 11(a)) drops rapidly from the maximum use of 46.1% to zero in four years. Figures 11(b)–11(d) show that Strategy J (blue dashed line) could provide a significant reduction in the number of infected dogs, infected livestock, and infected humans that deceases to the lower level $(I_d, I_l, I_h) = (6,16,5)$.

For Strategy K, all the controls u_1, u_2, u_3, and u_4 are considered in (17). The optimal controls u_1^*, u_2^*, u_3^*, and u_4^* are displayed in Figure 12(a). The control u_1^* (blue dash-dot line in Figure 11(a)) starts to have a 100% use for 12 years and then decreases gradually to zero. Both the control u_2^* (red dotted line in Figure 11(a)) and the control u_3^* (green dash-dot line in Figure 12(a)) have a 100% use for 10 years and then decline gradually to zero. Meanwhile, the control u_4^* (black dashed line in Figure 12(a)) drops rapidly from the maximum use of 46.1% to zero in four years. Figures 12(b)–12(d) show that Strategy K (blue dashed line) has a significant reduction in the number of infected dogs, infected livestock, and infected humans that could drop to the lower level $(I_d, I_l, I_h) = (6,15,5)$.

6. Conclusion and Discussion

This paper presents and analyzes a deterministic compartmental system for echinococcosis transmission dynamics under the intervention of constant slaughter inspection, anthelmintic treatment, environmental disinfection, and health education. The existence and stability of the disease-

free and disease-endemic equilibrium points of the model are discussed. It finds that the basic reproduction number determines entirely whether the disease is extinct or not endemic. In the absence of control measures, the basic reproduction number in Ganzi Tibetan Autonomous Prefecture is estimated to be $\mathcal{R}_0 = 1.0662 > 1$. This means that echinococcosis is an endemic disease. Craig et al. [13] stated that it is difficult to eliminate the spread of echinococcosis in scattered seminomadic remote communities, even if the Echinococcosis Control Program in Western China is carried out by using PZQ for the dog-dosing frequency monthly. Therefore, comprehensive interventions mainly including slaughter inspection, anthelmintic treatment, environmental disinfection, and health education should be taken into account to control the transmission of echinococcosis. Figures 2–12 have shown that the optimal strategies from Strategy A to Strategy K have a considerable significance in reducing the number of infected dogs, infected livestock, and infected humans. The combined prevention and control measures could eliminate the prevalence of echinococcosis.

Note that Strategies D, G, J, and K could reduce the number of infected dogs, infected livestock, and infected humans to a lower level than other strategies. Therefore, anthelmintic treatment and environmental disinfection may play a crucial role in controlling the number of infectious individuals. The anthelmintic treatment against echinococcosis does not eliminate the infection, and most of the time, when the treatments cease, there is a rebound in the infection (see [13]). Environmental disinfection may hence be indispensable for the prevention and control of echinococcosis. However, the importance of environmental disinfection for the prevention and control of echinococcosis is often ignored. Therefore, deworming and environmental disinfection should be the primary consideration in choosing control measures when developing an echinococcosis control and prevention program. The slaughter inspection with regard to meat inspection and offal disposal is aimed at reducing the number of infected dogs. Consequently, the number of EEs naturally decreases when the slaughter inspection is implemented. Thus, infected livestock would be reduced. From this perspective, the slaughter inspection may shorten the control time. The health education is aimed at reducing the possibility of ingestion by humans. The low evacuation rate of EEs would lead to the small possibility of ingestion by humans. Therefore, if the number of EEs drops to a certain level, the health education will become unimportant. That is to say that the health education has effectiveness in a short time for the prevention and control of echinococcosis. Hence, for faster and better prevention and control of echinococcosis, Strategy K may be recommended to be implemented in the real situation. Finally, some parameter values (for example, the death rate of EEs due to environmental disinfection) are not directly available; our model does not necessarily reflect the true picture of the prevalence of echinococcosis in the Ganzi Tibetan Autonomous Prefecture. Nevertheless, our model analysis suggests that environmental disinfection is critical to controlling the spread of echinococcosis and that the optimal integrated control strategy (Strategy K) can control the disease in the shortest possible time.

Appendix

A. Proof of Theorem 2

The Jacobian matrix of model (1) evaluated at E_{dfe} is obtained by

$$J = \begin{pmatrix} -\mu_d & \delta_d u_2 & 0 & 0 & -\frac{(1-u_1)\varepsilon\beta_d\Lambda_d}{\mu_d} & 0 & 0 & 0 \\ 0 & -(\mu_d+\delta_d u_2) & 0 & 0 & \frac{(1-u_1)\varepsilon\beta_d\Lambda_d}{\mu_d} & 0 & 0 & 0 \\ 0 & \gamma & -(\mu_x+c_h u_3) & 0 & 0 & 0 & 0 & 0 \\ 0 & 0 & -\frac{\beta_l\Lambda_l}{\varepsilon+\mu_l} & -(\varepsilon+\mu_l) & 0 & 0 & 0 & 0 \\ 0 & 0 & \frac{\beta_l\Lambda_l}{\varepsilon+\mu_l} & 0 & -(\varepsilon+\mu_l) & 0 & 0 & 0 \\ 0 & 0 & -\frac{(1-u_4)\beta_h\Lambda_h}{\mu_h} & 0 & 0 & -\mu_h & 0 & \delta_h \\ 0 & 0 & \frac{(1-u_4)\beta_h\Lambda_h}{\mu_h} & 0 & 0 & 0 & -(\omega+\mu_h) & 0 \\ 0 & 0 & 0 & 0 & 0 & 0 & \omega & -(\mu_h+\delta_h) \end{pmatrix}. \quad \text{(A.1)}$$

Then, the corresponding characteristic polynomial is

$$P(\lambda) = (\lambda + \mu_d)(\lambda + \mu_h)(\lambda + \varepsilon + \mu_l)(\lambda + \mu_h + \delta_h) \cdot (\lambda + \omega + \mu_h)\left(\lambda^3 + a_2\lambda^2 + a_1\lambda + a_0\right), \tag{A.2}$$

where

$$a_0 = (\varepsilon + \mu_l)(\mu_d + \delta_h u_2)(\mu_x + c_h u_3)\left(1 - \mathscr{R}_0^3\right),$$

$$a_1 = (\varepsilon + \mu_l)(\mu_d + \delta_h u_2) + (\mu_d + \delta_h u_2)(\mu_x + c_h u_3) + (\varepsilon + \mu_l)(\mu_x + c_h u_3),$$

$$a_2 = (\varepsilon + \mu_l) + (\mu_d + \delta_h u_2) + (\mu_x + c_h u_3). \tag{A.3}$$

Let $Q(\lambda) = \lambda^3 + a_2\lambda^2 + a_1\lambda + a_0$. It is evident from (A.3) that there are $a_1 > 0$ and $a_2 > 0$. If $\mathscr{R}_0 < 1$, then $a_0 > 0$. Furthermore,

$$a_1 a_2 - a_0 = [\mu_l + (\mu_d + \sigma u_2)]\left[a_1 + (\mu_x + c_h u_3)^2\right] + \mu_l(\mu_d + \sigma u_2)(\mu_x + c_h u_3)\mathscr{R}_0^3 > 0. \tag{A.4}$$

Using Routh–Hurwitz conditions [23], all roots of $Q(\lambda)$ have negative real parts. Then, it is clear that all roots of $P(\lambda)$ have negative real parts. Therefore, the disease-free equilibrium E_{dfe} is locally asymptotically stable when $\mathscr{R}_0 < 1$. By contrast, $Q(0) = a_0 < 0$ if $\mathscr{R}_0 > 1$. Since $\lim_{\lambda \longrightarrow +\infty} Q(\lambda) = +\infty$, there must be a positive root of $Q(\lambda)$ from the Intermediate Value Theorem. So, E_{dfe} is unstable if $\mathscr{R}_0 > 1$.

B. Proof of Theorem 3

It is worth noting that the first five equations of model (1) are independent of the last three equations of model (1). So, consider the first five equations of model (1) as a subsystem:

$$\begin{cases} \dot{S}_d = \Lambda_d - (1-u_1)\varepsilon\beta_d S_d I_l - \mu_d S_d + \delta_d u_2 I_d, \\ \dot{I}_d = (1-u_1)\varepsilon\beta_d S_d I_l - \mu_d I_d - \delta_d u_2 I_d, \\ \dot{X} = \gamma I_d - \mu_x X - c_h u_3 X, \\ \dot{S}_l = \Lambda_l - \beta_l S_l X - \varepsilon S_l - \mu_l S_l, \\ \dot{I}_l = \beta_l S_l X - \varepsilon I_l - \mu_l I_l. \end{cases} \tag{B.1}$$

Let $(S_d(t), I_d(t), X(t), S_l(t), I_l(t))$ be any solution of model (B.1) in Γ. This implies that $I_d(t) \le \Lambda_d/\mu_d$, $I_l(t) \le \Lambda_l/(\varepsilon + \mu_l)$ for all $t \ge 0$. Define a Lyapunov function as follows:

$$\mathscr{L}(I_d, X, I_l) = I_d + \frac{\mu_d + \delta_d u_2}{\gamma} X + \frac{(1-u_1)\varepsilon\beta_d\Lambda_d}{\mu_d(\varepsilon + \mu_l)} I_l. \tag{B.2}$$

Then, the derivative of $\mathscr{L}$ along the solutions of model (B.1) yields

$$\begin{aligned} \frac{d\mathscr{L}}{dt} &= \dot{I}_d + \frac{\mu_d + \delta_d u_2}{\gamma}\dot{X} + \frac{(1-u_1)\varepsilon\beta_d\Lambda_d}{\mu_d(\varepsilon + \mu_l)}\dot{I}_l \\ &= \left((1-u_1)\varepsilon\beta_d S_d - \frac{(1-u_1)\varepsilon\beta_d\Lambda_d}{\mu_d}\right) I_l \\ &\quad + \left(\frac{(1-u_1)\varepsilon\beta_d\beta_l\Lambda_d}{\mu_d(\varepsilon + \mu_l)} S_l - \frac{\mu_d + \delta_d u_2}{\gamma}(\mu_x + c_h u_3)\right) X \\ &\le \left(\frac{(1-u_1)\varepsilon\beta_d\beta_l\Lambda_d}{\mu_d(\varepsilon + \mu_l)}\frac{\Lambda_l}{(\varepsilon + \mu_l)} - \frac{\mu_d + \delta_d u_2}{\gamma}(\mu_x + c_h u_3)\right) X \\ &= \frac{\mu_d + \delta_d u_2}{\gamma}(\mu_x + c_h u_3)\left(\mathscr{R}_0^3 - 1\right) X. \end{aligned} \tag{B.3}$$

Therefore, $\dot{\mathscr{L}} < 0$ if $\mathscr{R}_0 < 1$ and $X > 0$. Moreover, $\dot{\mathscr{L}} = 0$ when $\mathscr{R}_0 < 1$ and $X = 0$. As a consequence, the only invariant set satisfying $\dot{\mathscr{L}} = 0$ is E_{dfe} when $\mathscr{R}_0 < 1$. By Lasalle's invariance principle [24], the disease-free equilibrium E_{dfe} is globally asymptotically stable if $\mathscr{R}_0 < 1$.

Now, consider the last three equations of model (1). From above, it has $\lim_{t \longrightarrow \infty} X(t) = 0$ if $\mathscr{R}_0 < 1$. So, it could be deduced that $\lim_{t \longrightarrow \infty} E_h(t) = 0$. Furthermore, $\lim_{t \longrightarrow \infty} I_h(t) = 0$ and $\lim_{t \longrightarrow \infty} S_h(t) = \Lambda_h/\mu_h$ could be derived. Thus, E_{dfe} is globally asymptotically stable for model (1) when $\mathscr{R}_0 < 1$.

C. Proof of Theorem 4

Since $\dot{S}_d + \dot{I}_d = \Lambda_d - \mu_d(S_d + I_d)$, and $\dot{S}_l + \dot{I}_l = \Lambda_l - (\varepsilon + \mu_l)(S_l + I_l)$, it implies that $\lim_{t \longrightarrow \infty}(S_d + I_d) = \Lambda_d/\mu_d$ and $\lim_{t \longrightarrow \infty}(S_l + I_l) = \Lambda_l/(\varepsilon + \mu_l)$. So the long-term dynamical behaviors of $S_d(t)$ and $S_l(t)$ could be replaced by $\Lambda_d/\mu_d - I_d(t)$ and $\Lambda_l/\mu_l - I_l(t)$, respectively. Consider the subsystem of model (1) as follows:

$$\begin{cases} \dot{I}_d = (1-u_1)\varepsilon\beta_d S_d I_l - \mu_d I_d - \delta_d u_2 I_d, \\ \dot{X} = \gamma I_d - \mu_e X - c_h u_3 X, \\ \dot{I}_l = \beta_l S_l X - \varepsilon I_l - \mu_l I_l. \end{cases} \tag{C.1}$$

Let

$$\Delta = \left\{(I_d, X, I_l) \in \mathbb{R}_+^3 : I_d \le \frac{\Lambda_d}{\mu_d}, X \le \frac{\gamma\Lambda_d}{\mu_d(\mu_x + c_h u_3)}, I_l \le \frac{\Lambda_l}{\varepsilon + \mu_l}\right\}. \tag{C.2}$$

The dynamics of model (C.1) can be focused on Δ since Γ is positively invariant for model (C.1). The method in [25] is adopted to explore the global stability of model (C.1). Define

$$h(\mathbf{v}) = \begin{pmatrix} h_1(v_1, v_2, v_3) \\ h_2(v_1, v_2, v_3) \\ h_3(v_1, v_2, v_3) \end{pmatrix} = \begin{pmatrix} -(\mu_d + \delta_d u_2)v_1 + (1-u_1)\varepsilon\beta_d\left(\frac{\Lambda_d}{\mu_d} - v_1\right)v_3 \\ -(\mu_x + c_h u_3)v_2 + \gamma v_1 \\ -(\varepsilon + \mu_l)v_3 + \beta_l\left(\frac{\Lambda_l}{\varepsilon + \mu_l} - v_3\right)v_2 \end{pmatrix}. \tag{C.3}$$

Then, $h : \mathbb{R}_+^3 \mapsto \mathbb{R}_+^3$ is a continuously differential map. It thus has $h(0) = 0$, and $h_i(\mathbf{v}) \geq 0$, $i = 1, 2, 3$, for all $\mathbf{v} \in \Delta$ when $v_i = 0$. Furthermore, $\partial h_i / \partial v_j \geq 0, i \neq j$, for $\mathbf{v} \in \Delta$, so that h is cooperative on Δ.

For $p \in (0, 1)$ and $\mathbf{v} \in \Delta$, it has

$$\begin{aligned} h_1(pv_1, pv_2, pv_3) &= -(\mu_d + \delta_d u_2)pv_1 + (1-u_1)\varepsilon\beta_d \\ &\quad \cdot \left(\frac{\Lambda_d}{\mu_d} - pv_1\right)pv_3 \geq -(\mu_d + \sigma u_2)pv_1 + \\ &\quad \cdot (1-u_1)\beta_d\left(\frac{\Lambda_d}{\mu_d} - v_1\right)pv_3 = ph_1 \\ &\quad \cdot (v_1, v_2, v_3). \end{aligned} \tag{C.4}$$

Similarly, it could be shown that $h_i(pv_1, pv_2, pv_3) \geq ph_i(v_1, v_2, v_3)$, $i = 2, 3$. So h is strictly sublinear on Δ.

By computing $Dh(\mathbf{v}) = (\partial h_i / \partial v_j)|_{1 \leq i,j \leq 3}$, it leads to

$$Dh(\mathbf{v}) = \begin{pmatrix} -(\mu_d + \delta_d u_2) - (1-u_1)\varepsilon\beta_d v_3 & 0 & (1-u_1)\varepsilon\beta_d\left(\frac{\Lambda_d}{\mu_d} - v_1\right) \\ \gamma & -(\mu_x + c_h u_3) & 0 \\ 0 & \beta_l\left(\frac{\Lambda_l}{\varepsilon + \mu_l} - v_3\right) & -(\varepsilon + \mu_l) - \beta_l v_2 \end{pmatrix}. \tag{C.5}$$

Then, $Dh(\mathbf{v})$ is irreducible on $\mathbf{v} \in \Delta$ because $|Dh(\mathbf{v})| \neq 0$. A straightforward computation shows that

$$Dh(0) = \begin{pmatrix} -(\mu_d + \delta_d u_2) & 0 & (1-u_1)\varepsilon\beta_d\frac{\Lambda_d}{\mu_d} \\ \gamma & -(\mu_x + c_h u_3) & 0 \\ 0 & \beta_l\frac{\Lambda_l}{\varepsilon + \mu_l} & -(\varepsilon + \mu_l) \end{pmatrix}. \tag{C.6}$$

Then, the characteristic polynomial of $Dh(0)$ is

$$Q(\lambda) = \lambda^3 + a_2\lambda^2 + a_1\lambda + a_0, \tag{C.7}$$

where a_0, a_1, and a_2 are known from (B.1). Then, $a_0 < 0$ when $\mathscr{R}_0 > 1$. According to the proof process of Theorem 3, there must exist a positive root of $Q(\lambda)$. Therefore, $s(Dh(0)) = \max\{\mathrm{Re}\,\lambda : Q(\lambda)\} > 0$. From Corollary 3.2 in [25], there are $\lim_{t\longrightarrow\infty} I_d(t) = I_d^*$, $\lim_{t\longrightarrow\infty} X(t) = X^*$, and $\lim_{t\longrightarrow\infty} I_l(t) = I_l^*$. Furthermore, $\lim_{t\longrightarrow\infty} S_d(t) = S_d^*$ and $\lim_{t\longrightarrow\infty} S_l(t) = S_l^*$.

When $\mathscr{R}_0 > 1$, the limiting system of the last three equations in model (1) is

$$\begin{cases} \dot{S}_h = \Lambda_h - (1-u_4)\beta_h S_h X^* - \mu_h S_h + \delta_h I_h, \\ \dot{E}_h = (1-u_4)\beta_h S_h X^* - \omega E_h - \mu_h E_h, \\ \dot{I}_h = \omega E_h - \mu_h I_h - \delta_h I_h. \end{cases} \tag{C.8}$$

It is evident that model (C.8) is linear. By computing the eigenvalues of the linear model (C.8), it could be shown that (S_h^*, E_h^*, I_h^*) is locally asymptotically stable. Therefore, (S_h^*, E_h^*, I_h^*) is globally asymptotically stable. According to [26], it concludes that the endemic equilibrium E_{ee} of model (1) is globally asymptotically stable.

Data Availability

The authors confirm that the data supporting the findings of this study are available within the article.

Conflicts of Interest

The authors declare that there are no conflicts of interest regarding the publication of this paper.

Acknowledgments

This work was supported by the National Natural Science Foundation of China (no. 11461058), Sichuan Minzu College (nos. XYZB2106ZB and XYZB2004ZA), and Science and Technology Bureau of Ganzi Tibetan Autonomous Prefecture (Project Name: Optimal Control Strategies for Echinococcosis Transmission Dynamics).

References

[1] *Echinococcosis fact sheet*, World Health Organization, 2020, https://www.who.int/news-room/fact-sheets/detail/echinococcosis.

[2] Centers for Disease Control and Prevention, "Parasites-echinococcosis," https://www.cdc.gov/parasites/echinococcosis/biology.html.

[3] M. G. Roberts, J. R. Lawson, and M. A. Gemmell, "Population dynamics in echinococcosis and cysticercosis: mathematical model of the life-cycle of Echinococcus granulosus," *Parasitology*, vol. 92, no. 3, pp. 621–641, 1986.

[4] M. G. Roberts, J. R. Lawson, and M. A. Gemmell, "Population dynamics in echinococcosis and cysticercosis: mathematical model of the life cycles of Taenia hydatigena and T. ovis," *Parasitology*, vol. 94, pp. 181–197, 1987.

[5] M. G. Roberts, "Modelling of parasitic populations: cestodes," *Veterinary Parasitology*, vol. 54, no. 1-3, pp. 145–160, 1994.

[6] Z. He, T. Yan, and Y. Yuan, "miRNAs and lncRNAs in Echinococcus and echinococcosis," *International Journal of Molecular Sciences*, vol. 21, p. 730, 2020.

[7] K. Wang, X. Zhang, Z. Jin, H. Ma, Z. Teng, and L. Wang, "Modeling and analysis of the transmission of echinococcosis with application to Xinjiang Uygur Autonomous Region of China," *Journal of Theoretical Biology*, vol. 333, pp. 78–90, 2013.

[8] L. Wu, B. Song, W. Du, and J. Lou, "Mathematical modelling and control of echinococcus in Qinghai province, China," *Mathematical Biosciences and Engineering*, vol. 10, no. 2, pp. 425–444, 2013.

[9] X. Rong, M. Fan, X. Sun, Y. Wang, and H. Zhu, "Impact of disposing stray dogs on risk assessment and control of echinococcosis in Inner Mongolia," *Mathematical Biosciences*, vol. 299, pp. 85–96, 2018.

[10] A. S. Hassan and J. M. W. Munganga, "Mathematical global dynamics and control strategies on Echinococcus multilocularis infection," *Computational and Mathematical Methods in Medicine*, vol. 2019, Article ID 3569528, 2019.

[11] G. Zhu, S. Chen, B. Shi, H. Qiu, and S. Xia, "Dynamics of echinococcosis transmission among multiple species and a case study in Xinjiang, China," *Chaos, Solitons & Fractals*, vol. 127, pp. 103–109, 2019.

[12] F. Tamarozzi, P. Deplazes, and A. Casulli, "Reinventing the wheel of Echinococcus granulosus sensu lato transmission to humans," *Trends in Parasitology*, vol. 2020, no. 36, pp. 427–434, 2020.

[13] P. S. Craig, D. Hegglin, M. W. Lightowlers, P. R. Torgerson, and Q. Wang, "Echinococcosis: control and prevention," *Advances in Parasitology*, vol. 96, pp. 55–158, 2017.

[14] J. Zhao and R. Yang, "A dynamical model of echinococcosis with optimal control and cost-effectiveness," *Nonlinear Analysis: Real World Applications*, vol. 62, article 103388, 2021.

[15] B. Buonomo and R. Della Marca, "Optimal bed net use for a dengue disease model with mosquito seasonal pattern," *Mathematical Methods in the Applied Sciences*, vol. 41, 2018.

[16] A. Lahrouz, H. El Mahjour, and A. Settati, "Dynamics and optimal control of a non-linear epidemic model with relapse and cure," *Physica A: Statistical Mechanics and its Applications*, vol. 496, pp. 299–317, 2018.

[17] X. Wang, M. Shen, Y. Xiao, and L. Rong, "Optimal control and cost-effectiveness analysis of a Zika virus infection model with comprehensive interventions," *Applied Mathematics and Computation*, vol. 359, pp. 165–185, 2019.

[18] M. A. Khan, S. W. Shah, S. Ullah, and J. F. Gómez-Aguilar, "A dynamical model of asymptomatic carrier zika virus with optimal control strategies," *Nonlinear Analysis: Real World Applications*, vol. 50, pp. 144–170, 2019.

[19] U. D. Purwati, F. Riyudha, and H. Tasman, "Optimal control of a discrete age-structured model for tuberculosis transmission," *Heliyon*, vol. 6, article e03030, 2020.

[20] I. A. Baba, R. A. Abdulkadir, and P. Esmaili, "Analysis of tuberculosis model with saturated incidence rate and optimal control," *Physica A: Statistical Mechanics and its Applications*, vol. 540, article 123237, 2020.

[21] E. O. Omondi, T. O. Orwa, and F. Nyabadza, "Application of optimal control to the onchocerciasis transmission model with treatment," *Mathematical Biosciences*, vol. 297, pp. 43–57, 2018.

[22] P. van den Driessche and J. Watmough, "Reproduction numbers and sub-threshold endemic equilibria for compartmental models of disease transmission," *Mathematical Biosciences*, vol. 180, no. 1–2, pp. 29–48, 2002.

[23] J. D. Murray, *Mathematical Biology I: An Introduction*, Springer, 3rd edition, 2002.

[24] J. P. Lasalle and S. Lefschetz, *Stability by Liapunov's Direct Method with Applications*, Academic Press, New York, 1961.

[25] X. Q. Zhao and Z. J. Jing, "Global asymptotic behavior in some cooperative systems of functional differential equations," *Canadian Applied Mathematics Quarterly*, vol. 4, no. 4, pp. 421–444, 1996.

[26] H. R. Thieme, "Convergence results and a Poincaré-Bendixson trichotomy for asymptotically autonomous differential equations," *Journal of Mathematical Biology*, vol. 30, no. 7, pp. 755–763, 1992.

[27] S. Lenhart and J. T. Workman, *Optimal Control Applied to Biological Models*, John Chapman and Hall, 2007.

[28] Statistics Bureau of Ganzi Tibetan Autonomous Prefecture, "Statistical bulletin of national economic and social development in Ganzi Prefecture," 2016, http://www.gzz.gov.cn/gzzrmzf/c100046/201703/df8104df6df341bbac7ef677fe7b4360.shtml.

[29] Statistics Bureau of Ganzi Tibetan Autonomous Prefecture, *Ganzi Prefecture Statistical Yearbook-2017*, Fangzhi Publishing House, 2018.

[30] T. Zou, "Grasp the key, break through difficulties and strengthen source control-Ganzi prefecture, Sichuan province hydatid disease prevention and control experience (Chinese)," *Zhongguo Dongwu Baojian*, vol. 7, pp. 58–62, 2017.